Case Studies in Construction Materials 20 (2024) e02929

Contents lists available at ScienceDirect

Case Studies in Construction Materials

journal homepage: www.elsevier.com/locate/cscm

Design considerations for eco-friendly palm-strand reinforced concrete for low-cost housing

Emmanuel Owoichoechi Momoh [a,*,1], Adelaja Israel Osofero [b,2], Oleksandr Menshykov [b,3]

[a] University of Exeter, Department of Engineering, Faculty of Environment, Science and Economy, Streatham Campus, Exeter EX4 4QF, United Kingdom

[b] University of Aberdeen, School of Engineering, King's College, Aberdeen AB24 3UE, United Kingdom

ARTICLE INFO

Keywords:
Carbon footprint
Concrete
Concrete Damage Plasticity
Developing countries
Finite element modelling
Housing
Palm fibres

ABSTRACT

Recent campaigns towards reducing the housing deficits and enhancing environmental sustainability in developing countries have led to increasing research efforts towards incorporating abundant natural materials into housing construction. One of such materials is oil palm broom fibres (OPBF) which began to attract research attention only recently for having the potential of being used as longitudinal reinforcement for concrete beams when combined as strands. This study provides some practical considerations and guidance for the design of OPBF-strand reinforced concrete using the flexural behaviour curves of 100 × 100 x 500 mm palm strand – reinforced prisms obtained from experimental investigation and parametric studies using finite element modelling. The study recommends the use of allowable stress design methodology for OPBF-strand reinforced concrete. A comparison of the carbon footprint between the OPBF- strand reinforced concrete beam and an equivalent steel reinforced concrete beam shows that the former could provide cheaper and eco-friendlier building material.

1. Introduction

Research on the incorporation of locally available wastes in building materials for the provision of infrastructure has gained significant attraction over the past three decades. For developing countries which are already plagued with huge infrastructure deficits, it is only reasonable to explore alternative construction and building materials that are affordable and sustainable. With a high population growth rate, increased rural-urban migration, lack of or difficulty in obtaining housing credit, and high inflation rates, securing decent accommodation is almost impossible for low and middle-income earners in these countries. For instance, Nigeria and India are each reported to have over 20 million housing units deficit [1]. In India, the bid to eliminate this housing deficit has also caused the increasing demand for conventional construction raw materials such as soil aggregates (which currently stand at 2 billion tonnes per annum) as well as increased importation of refined construction materials (e.g., steel), hence placing severe strain on the environment.

* Correspondence to: Harrison Building, Faculty of Environment, Science and Economy, University of Exeter, Streatham Campus, Room 252, Exeter, United Kingdom.
E-mail address: e.o.momoh@exeter.ac.uk (E.O. Momoh).
[1] https://orcid.org/0000-0003-3432-1366
[2] https://orcid.org/0000-0002-5476-5979
[3] https://orcid.org/0000-0003-2869-3307

https://doi.org/10.1016/j.cscm.2024.e02929
Received 26 July 2023; Received in revised form 23 December 2023; Accepted 27 January 2024
Available online 1 February 2024

Nomenclature

ε_{cu}	is the maximum strain of concrete in uniaxial compression
ε	is the strain
ε_{cs}	is the free shrinkage strain
$E_{concrete}$	is the Young's modulus of the concrete
E_{opbf}	is the Young's modulus of OPBF strands
E_{steel}	is the Young's modulus of steel reinforcement
$E_{c,eff}$	is the effective Young's modulus of concrete
n	is the modular ratio
n_e	is the effective modular ratio
A_T	is the area of steel reinforcement
A_f	is the area of OPBF strand reinforcement
M	is the moment capacity of section
r	is the radius of curvature
$1/r$	is the total curvature
$1/r_{cs}$	is the curvature due to shrinkage
$1/r_{cs(un)}$	is the curvature due to shrinkage of the uncracked section
$1/r_c$	is the curvature due to creep of the section
k	is the deflection constant
$\delta_{\max}$	is the maximum midspan deflection
w	is the uniformly distributed load
ξ	is the distribution coefficient
β	is the load duration factor
σ_s	is the stress in the tension steel for the cracked concrete section
σ_{sr}	is stress in the tension steel calculated based on a cracked section
σ_i^D	is the contact stress after damage initiation
d_{Tf}	is the tension damage parameter for OPBF strand
d_{cf}	is the compression damage parameter for OPBF strand
$\sigma_i^{'}$	is the contact traction at normal and shear directions (i)
f_t	is the uniaxial tensile strength of concrete
f_{cu}	is the maximum uniaxial compressive strength of concrete
f_{cm}	is the mean concrete strength in uniaxial compression
f_{tu}	is the maximum uniaxial tensile strength of concrete
ε_{cu}	is the maximum strain of concrete in uniaxial compression
$\varepsilon_o^{'}$	is strain of concrete at maximum uniaxial compressive stress f_{cu}
ε_o^{el}	is elastic strain of concrete in uniaxial compression
ε_{of}^{el}	is the elastic strain of OPBF strand in tension
ε_f^{in}	is the inelastic strain of OPBF strand in tension
ε^{in}	is the inelastic strain of concrete
E_o	is the undamaged elastic stiffness of concrete
E_{of}	is the undamaged elastic stiffness of OPBF strand
E_{fc}	is the damaged stiffness of OPBF strand in compression
d_c	is the compression damage parameter of concrete
d_t	is the tension damage parameter of concrete
ε_t	is the tensile strain of concrete
ε_{cr}	is the cracking strain
ϵ	is the eccentricity
ψ	is the dilation angle of material
f_{bo}	is the concrete strength in biaxial compression
f_f	is the uniaxial tensile strength of OPBF strand
f_{fT}	is the maximum uniaxial tensile strength of OPBF strand
f_{fTd}	is the design tensile strength of OPBF strand
f_{fc}	is the maximum compressive strength of OPBF strand
f_{yd}	is the design strength of the steel reinforcement
ε_T	is the tensile strain at f_{fT}
ε_T^{in}	is the inelastic strain of OPBF in uniaxial tension
ε_c^{in}	is the inelastic strain of OPBF in uniaxial compression
ε_{cT}	is the total compressive strain of OPBF strand

ε_{of}^{el}	is the elastic strain of OPBF in uniaxial tension
ε_{oc}^{el}	is the elastic strain of OPBF in uniaxial compression
E_{oc}	is the undamaged elastic compressive stiffness of OPBF strand
E_f	is the post-elastic stiffness of the OPBF strand in tension
d_{Tf}	is the tension damage parameter of OPBF strand
d_{cT}	is the compression damage parameter of OPBF strand
k_{nn}	is the cohesive stiffness in the normal direction
k_{ss}	is the cohesive stiffness in the shear direction
k_{tt}	is the cohesive stiffness in the tangential direction
d_x	is the effective depth of reinforcement
M	is the moment capacity of section
ϕ	is the creep coefficient
S	is the first moment of area of reinforcement about the centroid of the section
I	is the second moment of area of section
I_{cr}	is the second moment of area of the cracked section
A_T	is the area of OPBF strand reinforcement
ρ	is the reinforcement ratio
b	is the breadth of the section
d_e	is the effective depth of the section
D	is the damage evolution parameter
F_c	is the compressive force in concrete
f_{cu}	is the compressive stress in concrete
α	is the neutral axis depth factor
x	is the depth of the neutral axis
f_T	is the tensile stress in the strand reinforcement
sc	is spacing between reinforcement bars
h	is the overall height of the section
h_o	is the notional size of the beam
$\Phi_{stirrup}$	is the diameter of stirrup
Φ_{rebar}	is the diameter of reinforcement bar
Φ_T	is the diameter of OPBF strand
$V_{Rd,max}$	is the shear demand at the face of the beam
V_{Ed}	is the design shear force
A_c	is the gross area of the section
k_h	is the coefficient depending on the notional size of the section
ε_{cd}	is the drying shrinkage strain
$\varepsilon_{\mathrm{ca}}$	is the autogenous shrinkage strain
t	is the present age of the concrete in *days*
t_s	is the age of the concrete (days) at the beginning of drying shrinkage (or swelling)
f	is the allowable material strength
u	is the exposed perimeter of the section
q	is the number of strands per layer of reinforcement
α, β, γ, λ_1 and λ_2	are the constants of OPBF strand stress-strain constitutive behaviour

The negative environmental impact comes in the form of the removal of the vegetative cover from the quarry area resulting in soil erosion, not to mention the carbon emission from quarry activities such as ore/aggregate mining, crushing and transportation.

The increasing levels of CO_2 in the atmosphere require urgent attention from all stakeholders in the construction industry. The building sector consumes over 40% of the total world energy, 25% of the global water resources, 40% of the total global resources and is responsible for about 33% of the global emission of greenhouse gases [2,3]. Carbon emission from quarrying activities alone is reported to produce about 20 kg of CO_2 per 100 kg of aggregate [4]. Despite these glaring statistics, energy expenditure put into the manufacture of conventional construction materials and building components has also been on the increase [3,5,6]. Therefore the careful selection of alternative sustainable building materials cannot be overemphasised [2] and hence the need to re-use waste materials or source new materials which are renewable, environmentally sustainable and that require less energy in their manufacture [7,8]. This is especially true for developing countries which are already plagued with huge infrastructure deficits [9,10]. Fortunately, the enormous amounts of concrete wastes and other solid wastes generated annually in these developing countries if properly harnessed could translate into viable building materials that are not only cheap but also provide more environmentally friendly options [11,12]. Research on the incorporation of locally available building materials in the provision of infrastructure has gained significant attraction over the past three decades. Such materials include solid wastes from construction, agriculture, manufacturing industries, and municipal life, such as demolition wastes, rubber wastes [12], antimony tailings [13], municipal solid wastes, plastic wastes [14], agricultural biomass, etc.

The agricultural sector accounts for a significant amount of annual global solid waste generation with a more than 300% increase in biomass generation in the last 50 years which is expected to continue to rise as the world's population exceeds 10 billion by 2050 [4]. Hence management of waste biomass continues to pose challenges,especially in developing countries [15]. In an attempt to get rid of the waste, an uncontrolled open-burning technique is employed which leaves a large carbon footprint in the environment [1,4,16,17]. Waste biomasses include natural fibres which has been used, in the form of straw, for reinforcing clay bricks since ancient times [18]. However, research on the incorporation of natural fibres in concrete only started in the 1940 s [19,20]. Since then, substantial investigations have been carried out on the material properties of numerous natural fibres as well as on associated merits and demerits of their application in construction [3]. Their availability at low cost in many countries around the world, and the recent drive towards environmental conservation has led to the increase of research activities towards incorporating them in concrete and cement composites, together with increase in demand for building components made of natural fibre-reinforced cement composites [3,19,21]. The demand is due to their lightweight, reduced thermal conductivity, improved acoustic insulation and economic feasibility. Some of these components are in the form of cementitious roofing panel and claddings [2,22,23], building insulation [17,24], self-compacting mortar [21,25,26], polymer composites [27–29], and concrete pavements [3].

Natural fibres that have attracted research attention include (but not limited to) hemp, straw, flax, bamboo, animal hair, cork, coir, jute, pineapple leaves, bamboo, banana, cotton, sugarcane, grasses, and palms. The incorporation of these fibres has been reported to improve the durability and mechanical properties of concrete and other cementitious composites [14,30,31]. Arun et al. [17] also reported a 23% savings in cost by partially replacing cement and coarse aggregates with 15% and 20% fly ash and coconut shell respectively in geogrid slabs as an alternative to expanded polystyrene geogrid slab. While wastes such as shells, husks and fibres have been used largely for the provision of discrete reinforcement in concrete, their use as longitudinal reinforcement is non-existent except for bamboo culms and, only recently, broom strands from oil palm tree.

1.1. Use of OPBF in concrete

The oil palm tree (*Elaeis guineensis*) is a conglomeration of natural fibre biomass and as such, waste disposal problems exist in countries with the highest cultivation of oil palm trees such as Indonesia, Malaysia, Thailand, Nigeria, and Columbia [9,32,33]. Total waste biomass generation from oil palm cultivation activities in Malaysia alone stands at 21.03 million tonnes of pruned fronds, 7.34 million tonnes of empty fruit bunches, 4.46 million tonnes of kernel shells and 7.72 million tonnes of mesocarp fibres [32]. These oil palm biomasses have attracted enormous research attention except for the leaflet ribs popularly referred to as oil palm broom fibres (OPBF). Furthermore, while plant wastes such as shells, husks and fibres have been used largely for the provision of discrete reinforcement in concrete, their use as longitudinal reinforcement is non-existent except for bamboo culms [34,35] and only recently, OPBF [9,36].

Until recently, bamboo was the only plant widely studied as longitudinal reinforcement in concrete. The use of broom fibres (or briskets) from oil palm leaflets as reinforcement for cementitious composites was firstly mentioned in the study of Momoh and Dahunsi [37] where the broom fibres were weaved in form of meshes and embedded in laterite-based roof tiles as reinforcements. The study reported over 100% improvement in the flexural capacity of the broom-reinforced roof tiles. This motivated a further study [38] which provided a characterisation of the OPBF and reported an average tensile strength of 389 MPa. Like bamboo, OPBF was discovered to have a tensile strength-to-weight ratio of about 5 times that of steel [38]. The use of OPBF in the form of small discrete (50 mm) fibres as randomly distributed reinforcement in concrete was later studied. Although there were no improvements in the mechanical properties of the 30 MPa concrete, over 400% increase in flexural toughness was recorded, thereby signalling the possible use of OPBF-concrete as a low-cost building material for developing countries in seismic regions [39]. Following this study, the bond pull-out behaviour of OPBF from concrete was investigated with maximum bond strengths of 1.16, 0.95 and 0.82 MPa recorded at 28, 56 and 112 days, respectively [40]. The degradation of bond strength with time was traced to cement alkali-embrittlement of the OPBF surface at the interface. A subsequent study investigated possible solutions to the alkali-induced fibre surface degradation by investigating different pre-treatment techniques for the OPBF. The recommended treatment techniques include soaking the OPBF in either 6% NaOH solution at 48 h at room temperature, or 3% silane for 24 h at room temperature or in hot water (at 100 ^{0}C) for 30 min with the tensile strength of the OPBF increased by more than 30% [41]. Consequently, the embrittlement of the fibres in concrete was also mitigated

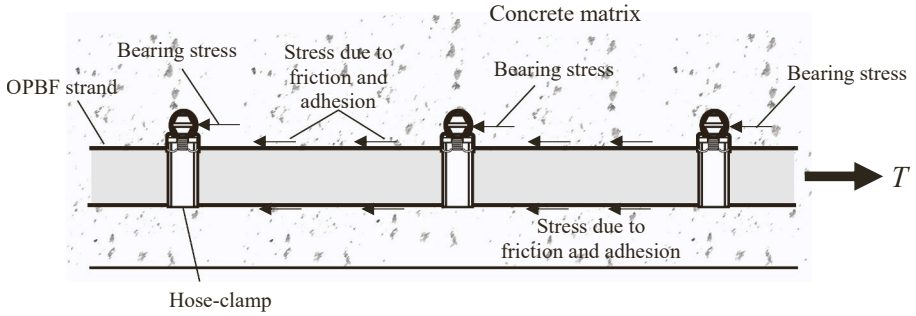

Fig. 1. Simplified conceptualisation of bond stress distribution for hose-clamp fitted reinforcement strand in concrete [36].

and the bond strength between the OPBF strands and concrete was improved for randomly dispersed fibre reinforcement [42].

However, the reported pre-treatment methods may not suffice should the OPBF strands be used as longitudinal reinforcement for concrete. This is because of the slippage between fibres within the strands, hence causing the failure of the reinforcing strands to act monolithically. Therefore, the use of hose clamps was employed in combining the OPBF into strands prior to their use as longitudinal reinforcement in concrete beams [39]. A schematic representation of a hose-clamp actualised broom strand reinforcement in concrete matrix is shown in Fig. 1. Aside from the hose clamps aiding the monolithic action of the strand, they also provided shear locking between the concrete and the reinforcement thereby improving bond strength as well as the overall flexural capacity of the composite. The use of hose-clamps to enhance the monolithic action of the OPBF reinforcement strands was implemented in the study of Momoh et al. [36]. The flexural behaviours of unreinforced concrete, OPBF reinforced concrete (OPBF-RC) and steel reinforced concrete (SRC) prisms were analysed, and recommendations were made for the minimum reinforcement ratio of OPBF longitudinal reinforcement for lightly loaded beams. Factors such as the relatively low elastic modulus and unique tensile behaviour of the OPBF strands were responsible for the increased deflection of the natural fibre-reinforced prisms. The study recommended the use of palm strand reinforced concrete for building elements under light structural demands like lintels of low-cost residential houses.

1.2. Study significance

Although OPBF strand reinforced concrete is recommended for light beams [36], analysis of practical factors and bespoke considerations affecting the structural design of this unfamiliar composite is lacking. Such factors include the pseudo-plastic tensile behaviour of the OPBF strands as well as the imperfect bond between the strand reinforcement and concrete. An understanding of these factors is imperative and would help in the formulation of design guidance and recommendations for the natural fibre-reinforced concrete beams in ultimate and serviceability limit states. To achieve this aim, the philosophy behind steel reinforced concrete is discussed and modified to derive adequate procedures for the design of OPBF-strand reinforced concrete (OPBF-RC). Furthermore, design examples are considered and a comparative analysis of carbon footprints between each designed OPBF-RC section and an equivalent SRC section is presented.

2. OPBF-strand reinforced concrete

2.1. Flexural behaviour

All OPBF were dried to a moisture content of less than 10% with each broom brisket visually inspected to ensure that they were free of any defects or damage. The reinforcement strands were then produced by combining individual broom briskets and holding them in position by steel hose clamps spaced at specified distances along each strand and tightened to a torque of 3.5 N-m. The samples tested include an unreinforced concrete prism, a steel reinforced concrete prism and 6 palm strand reinforced concrete prisms. All prisms were of 100 $\times$ 100 x 500 mm dimension while the concrete was grade C30. The reinforced samples were singly reinforced with two bars of the respective material and without shear reinforcement (stirrups). For the OPBF-RC samples, the sample identification reveals the number of OPBF in each strand, and the spacing of the hose clamps, such that, 120 F-45 s for instance refers to a sample consisting of 120 fibres with hose clamps spaced at 45 mm centre-to-centre. Fig. 2 presents (a) the steel 6 mm diameter steel reinforcement, (b) a 120 F-85 s OPBF-strand reinforcement, (c) a 120 F-85 s OPBF-strand reinforcement placed in a mould, and (d) sections of the prisms, Fig. 3 shows a typical tensile and compressive stress-strain curve of an OPBF reinforcement strand with some stress-strain curves for bamboo and steel for comparison. Fig. 4 shows the 28 days flexural response of unreinforced, SRC and 100 $\times$ 100 x 500 mm hose-clamp enhanced OPBF-RC prisms. Details of the test procedures can be found in the study of Momoh et al. [36].

The tensile response of the OPBF-strand begins with a linear elastic regime until a stress of about 65 MPa after which fibres within the strand begin to fail thereby leading to a reduction in the elastic modulus until sudden failure occurs at a maximum stress of 200 MPa. This pseudo-plastic behaviour is unlike the linear elastic and sudden failure for bamboo culms used as similar longitudinal reinforcement for concrete [34,35,48]. The pseudo-plastic behaviour of the natural fibre reinforcement is beneficial for the gradual failure of the OPBF-RC [9,36]. From Fig. 4, the maximum flexural capacity of the 120 F-45 s sample (reinforcement ratio of 3.49%) can be approximated to be equal to the maximum flexural capacity of the steel-reinforced concrete (reinforcement ratio of 0.56%). However, the maximum flexural capacity of the steel reinforced concrete is reached before 1 mm deflection as against over 3 mm deflection for the OBFF-RC thereby indicating potential serviceability concerns. Furthermore, the serviceability limit of deflection for steel reinforced concrete beams is measured by comparing the calculated span/effective depth ratio with the specified limit in Eurocode 2 [49].

Although the span/effective depth ratios for the samples whose flexural responses are presented in Fig. 4 satisfy the code requirement, the sample dimensions (100 x 100 x 500 mm) may be too small to make recommendations especially on a new reinforcement type like the clamp-enhanced OPBF-strands. Generally, the code provides for the maximum deflection limit of 0.4% of the span which translates to the deflection limit of 1.8 mm for the 450 mm span of the samples tested in the experiments. While the steel reinforced sample clearly reaches its peak strength before the deflection limit, the OPBF-strand reinforced samples achieved only about 65% of their maximum capacity. Considering the differences in elastic moduli (between OPBF strands and steel) as well as relatively low bond strength between OPBF and concrete, a fundamental understanding of reinforced concrete design is needed in order to make practical design decisions for OPBF-RC beams.

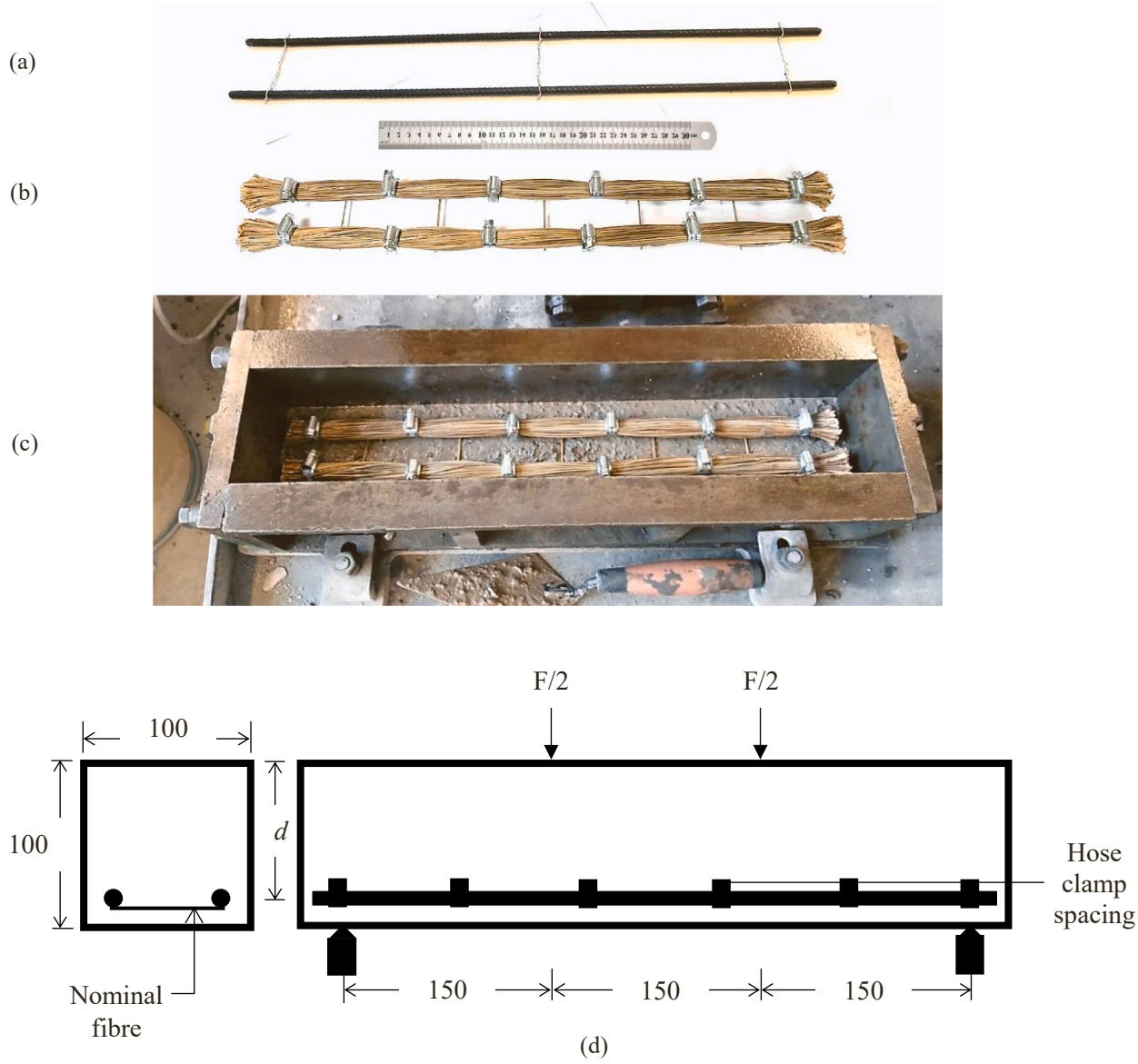

Fig. 2. (a) 6 mm Ø steel reinforcement (b) a 120 F-85 s OPBF-strand reinforcement (c) OPBF reinforcement placed in 100 × 100 x 500 mm mould (d) cross-section and longitudinal section of sample.

2.2. Design philosophy

Unlike steel, concrete possesses poor resistance in tension. Therefore, the concept of reinforcing concrete with steel is such that the steel is placed in the region of the concrete matrix where tensile stresses are predominant while the concrete is apportioned to resist compressive stresses. Hence for steel-reinforced concrete, the section is provided with an area of reinforcement to ensure that the reinforcement yields before concrete crushes in compression so that the section fails gradually in a ductile manner. The ductility of steel is therefore important to avoid sudden tensile failure [50,51].

In any reinforced concrete structural element, the section is designed using the principles of, (1) equilibrium, and (2) strain compatibility. From Fig. 1, consider force (T) in the reinforcement at a strain which is below 0.0035 (the crushing strain of concrete), the force (T) is given as the product of the area of the reinforcement (A) and the stress (f) in the reinforcement. In other words

$$T = area\ (A)\ \text{x}\ stress\ (f) \tag{1}$$

Eq. 1 may be more accurately written as

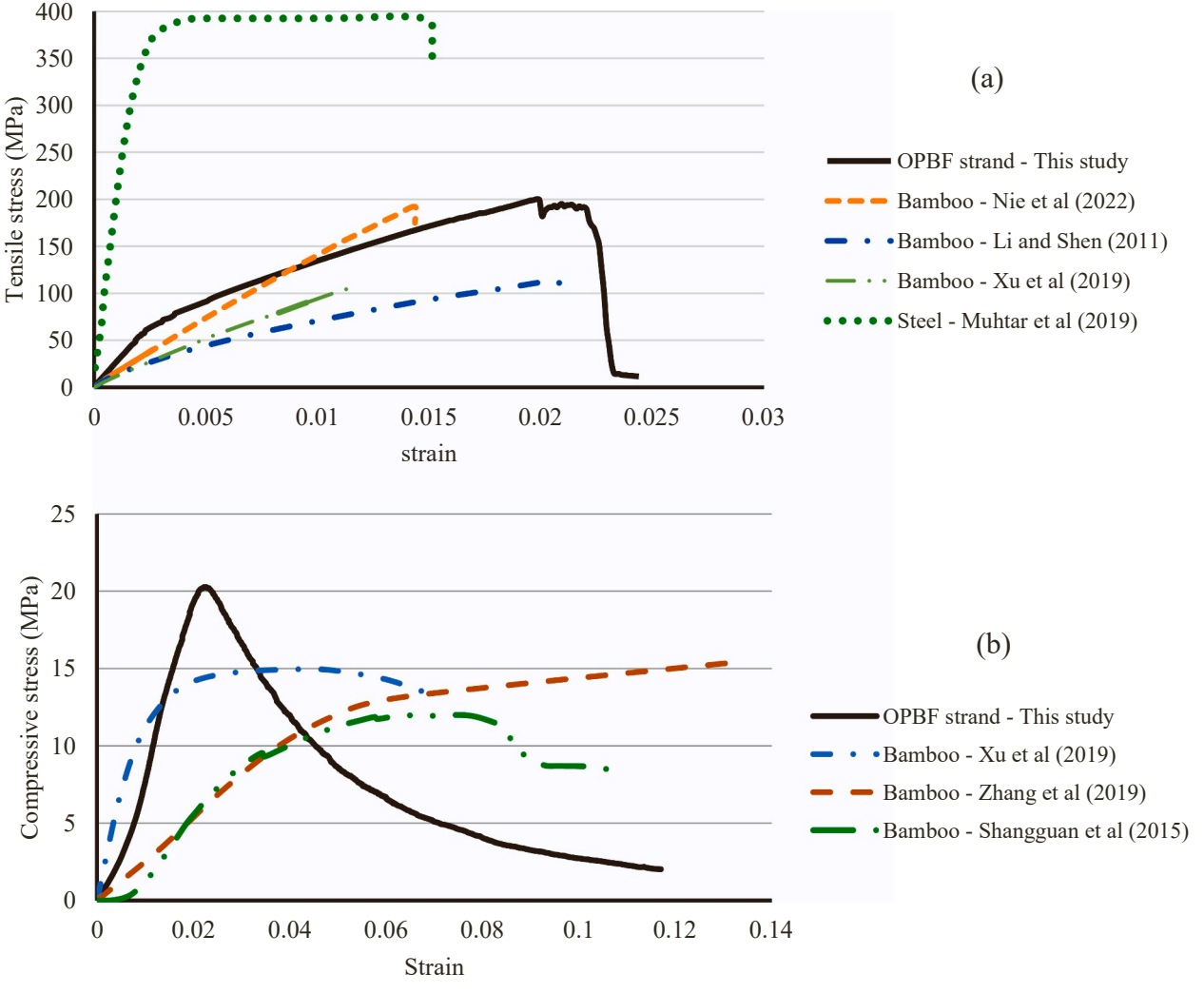

Fig. 3. (a) Tensile and (b) compressive stress-strain curve of a typical OPBF strand in comparison with steel and bamboo [43–47].

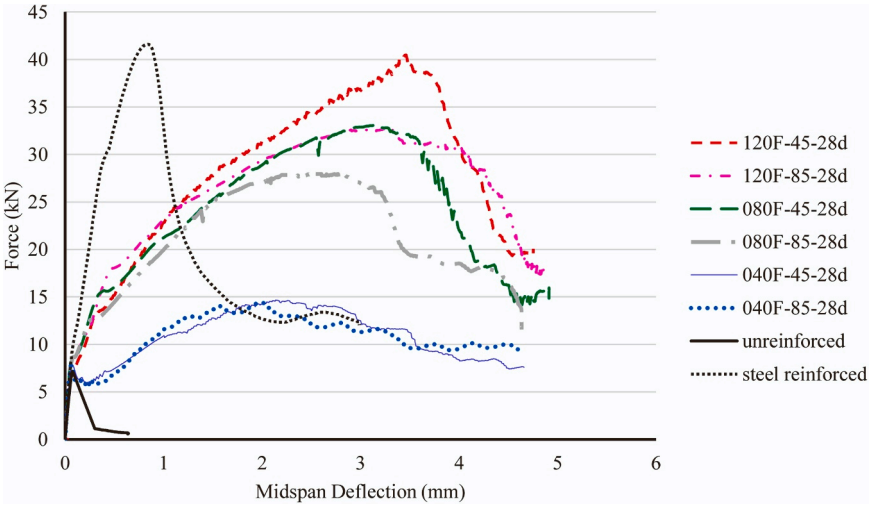

Fig. 4. Flexural response of clamp enhanced OPBF reinforced concrete at 28 days [36].

$$T = area\ (A)\ \text{x}\ strain\ (\varepsilon)\ \text{x}\ Young's\ modulus\ (E) \tag{2}$$

The implication of Eq. 2 is that, for the equivalent force in steel reinforced concrete (T) to be developed in OPBF-RC, the area of OPBF-strand reinforcement (A_T) needs to be increased due to the relatively lower elastic modulus of OPBF. The proportion to which A_T needs to be increased depends on the steel – OPBF modular ratio (n). The modular ratio can be defined as:

$$n = \frac{E_{steel}}{E_{opbf}} \tag{3}$$

From the study of Momoh et al. [36], the elastic modulus of the OPBF-strand (E_{opbf}) is about 26 GPa. Adopting a range of 20 – 26 GPa results in a range of modular ratio of 7.7 – 10. On the other hand, a larger value of T can be obtained by allowing a larger strain (ε) value, but serviceability requirements of deflection and cracking would not be satisfied. So, the reasonable option would be to increase the value of A_T. The area of OPBF reinforcement A_T can be increased by adding more layers of OPBF reinforcement, but again, there is a concern. Adding more layers of the OPBF reinforcement reduces the depth of the neutral axis which means that the effect of A_T on developing the full magnitude of T may be reduced especially as reinforcement layers closer to the neutral axis may not be fully mobilised.

For serviceability, Eq. 2 can be viewed in terms of the axial stiffness of the reinforcing material by keeping the strain constant such that:

$$T = \varepsilon\ \text{x}\ A_T E\cdot \tag{4}$$

Here the axial stiffness term $A_T E$ provides the bridging action against cracks and hence controls deflection of the structural element. To achieve a commensurate performance of SRC, i.e., by reducing deflection and cracks, again, A_T needs to be increased. The maximum limit to which A_T can be increased would determine the limits of the reinforcement ratio.

For conventional SRC, the limits of reinforcement for a given section are specified to enhance the yielding of the reinforcement, thereby avoiding sudden brittle failure of the SRC composite. By so doing, the reinforcement creates redistribution of the stress in the concrete which delays localised cracking, and as a consequence, sudden brittle failure of the composite is prevented. In Eurocode 2 [49], the required minimum reinforcement for a steel reinforced section is 0.13% of the cross-sectional area. From preliminary findings shown in Fig. 4, at the ultimate limit state of maximum flexural capacity of 40 kN, the reinforcement ratio of the OPBF-RC section was 3.49% (i.e., the 120 F-45–28d sample), while that of the SRC section was 0.56%. In other words, to achieve a maximum capacity of 40 kN, the OPBF reinforcement ratio should be set to 3.49%. Similarly, an equivalent load capacity would be achieved with a steel reinforcement ratio of 0.56%. By direct proportion, the minimum reinforcement ratio of 0.13% stipulated by Eurocode 2 [49] for SRC sections would translate to a minimum reinforcement ratio of 0.81% for OPBF-strands sections. However, after careful consideration of Fig. 4, this study recommends a minimum reinforcement ratio of 2.33% for OPBF-strands (i.e., the 080 F samples) to avoid excessive localised cracking. The difference between the minimum reinforcement ratios by direct proportion and the recommendation from the experimental results of this study can be traced to the relatively low bond strength between the OPBF reinforcement and concrete. In a comparison presented in the previous study [40], the 28 days bond strength between plain OPBF strands with 80 mm embedded length is about 40% of the 28 days bond strength of TMT steel with 150 mm embedded length reported in the study of Kute and Wakchaure [52]. For clamp-enhanced OPBF-strands, results show a maximum bond strength of 1.6 MPa for an embedded length of 80 mm. This bond strength is about 55.7% of that of steel reinforcement bars with concrete reported in the study [40]. Clearly, reduced bond strength would require the value of A_T to be further increased if the performance of the section in terms of serviceability is to match an

equivalent SRC section. Concerns around bond stress also imply that the usual strain compatibility conditions assumed for SRC may not apply.

Other significant problems that would arise with an increase in A_T (in a bid to adopt a steel reinforcement concrete approach) are:

- difficulty in reinforcement detailing and,
- difficulty in controlling excessive localised cracking, especially because OPBF reinforcement is of a lower modulus of elasticity than concrete. This implies that concrete would firstly crack before stress is transferred onto the reinforcing OPBF-strands.

Consequently, a *Hybrid Section* consisting of OPBF longitudinal reinforcement and conventional steel stirrup is recommended. It is asserted that the steel stirrups would be effective against shear cracks and deflection. Secondly, an Allowable Stress Design methodology is proposed for the ultimate limit state while a detailed analysis is required for deflection checks. Higher deflections for the natural strand reinforced concrete implies that an in-depth analysis of deflection is required because deflection will be critical to the design.

3. Design of OPBF reinforced concrete beams

3.1. Serviceability limit state

3.1.1. Deflection calculation

Eurocode 2 [49] provides guidelines on how to satisfy the serviceability limit state of deflection by either direct calculation or by providing for a specific limit of span/effective depth ratio. The latter method is easier and widely used with SRC but may not be suitable for OPBF-RC due to the following reasons:

- From Table 7.4 N of Eurocode 2, the definitions of "highly stressed" and "lightly stressed" concrete may not apply to OPBF-RC due to the relatively lower elastic modulus of the OPBF strands, lack of strain compatibility between concrete and reinforcement, and the relatively lower bond strength at the OPBF-concrete interface. Hence the span/effective depth limits specified for each class may not suffice.
- The specification of span/effective depth limit as a condition for deflection for SRC is borne out of robust data from numerous experiments and parametric studies spanning hundreds of years. Studies on OPBF-RC are very recent with limited data available.

Due to the nascent stage of the study of OPBF-RC, an allowable stress method is proposed, and a direct calculation of actual deflections of the OPBF-RC beams is recommended. Deflection calculation is carried out to determine the curvature of sections under loading with respect to creep and shrinkage.

Consider the idealised beam of span (L) pinned-supported at both ends with a constant moment M over the whole span in Fig. 5. Under the elastic beam theory,

$$M_x = EI\frac{d^2y}{dx^2} \tag{5}$$

while deflection (δ) at any section can be given by:

$$\delta = \frac{M}{EI}\left(\frac{x^2}{2} - \frac{Lx}{2}\right) \tag{6}$$

At midspan (i.e., at $x = L/2$) the maximum deflection is given by:

$$\delta_{\max} = \frac{M}{EI}\quad\left(-\frac{L^2}{8}\right) \tag{7}$$

Recall that curvature ($1/r$) can be expressed as:

$$\frac{1}{r} = \frac{M}{EI} \tag{8}$$

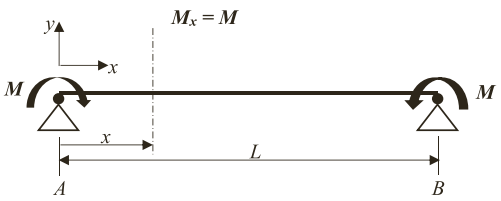

Fig. 5. Idealised pin-ended beam with constant moment.

Substituting Eq. 8 in Eq. 7, the maximum deflection can be generally written as:

$$\delta_{max} = \frac{1}{r} \quad kL^2 \tag{9}$$

where k is a constant determined from the loading scenario and in this case, $k = 0.125$. Eq. 9 is a generic expression for deflection which is handy as soon as the value of k is determined. For example, the maximum deflection of a simply supported beam of span (L) loaded throughout the span with a uniformly distributed load (w) is given as:

$$\delta_{max} = \frac{5wL^4}{384EI} \tag{10a}$$

Eq. 10(a) contains the maximum moment (M) occurring at midspan which is given as:

$$M = \frac{wL^2}{8} \tag{10b}$$

Expressing Eq. 10(a) in form of the generic Eq. 9 gives:

$$\delta_{max} = \frac{wL^2}{8EI} \text{ x } \frac{5}{48} \text{ x } L^2 \tag{10c}$$

From the right side of Eq. 10(c), the value of k is 5/48 or 0.104. Similarly, the k value of any loading arrangement on a beam can be determined from its maximum deflection equation.

The general limits for deflection provided in Eurocode 2 [49] are:

(a) Span/250 for beams, slabs, or cantilevers.
(b) Part of deflection that occurs as a result of applying finishes or partitions should not exceed span/500.

These provisions ensure that it is accurate to use the average curvature of the cracked and uncracked sections.

3.1.2. Calculation of curvature

Section 7.4.3 (3) of Eurocode 2 [49] requires that any one of the three deformation parameters of strain, curvature or rotation must be determined. In this study, curvature is the chosen deformation parameter due to its ease of determination. Eurocode 2 requires that the curvatures of the section in both its cracked and uncracked states are calculated. Then an estimate of the average value of curvature is obtained using Eq. 11 [49]:

$$\frac{1}{r} = \xi \left(\frac{1}{r}\right)_{cr} + (1 - \xi) \left(\frac{1}{r}\right)_{uc} \tag{11}$$

where $1/r$ is the *average curvature*, ξ is a *distribution coefficient* given by $1 - \beta(\sigma_{sr}/\sigma_s)^2$ allowing for tension stiffening, and β is the *load duration factor* (1 for short term load; 0.5 for sustained loads or cyclic loading). Eurocode 2 states that the parameter (σ_{sr}/σ_s) can be replaced by M_{cr}/M, where σ_s is the *stress in the tension steel for the cracked concrete section*, and σ_{sr} is the *stress in the tension steel calculated based on a cracked section under the loading that will just cause cracking of the section*. It is necessary to calculate the average value of both the cracked and uncracked sections because although cracks are inevitable for most concrete beams, the member may not behave as a fully cracked section.

3.1.3. Curvature due to creep and shrinkage

Creep will increase deflection with time, so an effective Young's modulus of concrete $E_{c,eff}$ is used for the calculation:

$$E_{c,eff} = \frac{E_{cm}}{(1 + \phi(\infty, t_0))} \tag{12}$$

Where ϕ is the *creep coefficient* (i.e., creep strain/initial elastic strain). Typical values of the creep coefficient are provided in Eurocode 2. In like manner, the effects of shrinkage will increase the deflection. Curvature due to shrinkage ($1/r_{cs}$) is given by

$$\frac{1}{r_{cs}} = \frac{\varepsilon_{cs}\alpha_e S}{I} \tag{13}$$

where ε_{cs} is the free shrinkage strain, S is the first moment of area of reinforcement about the centroid of the section, I is the second moment of area of section (whether cracked or uncracked, whichever is appropriate, and n_e is the effective modular ratio ($E_s/E_{c,eff}$).

The procedure for the calculation of deflection can therefore be summarised below:

- ***Creep due to loading***

  - Calculate curvature due to uncracked section

- Calculate curvature due to cracked section
- Calculate the average of the cracked and uncracked curvature (i.e., average curvature).

- ***Shrinkage due to loading***

- Calculate curvature due to uncracked section
- Calculate curvature due to cracked section
- Calculate the average of the cracked and uncracked curvature (i.e., average curvature)

- ***Calculate deflection***

Deflection = (*curvature due to loading* + *curvature due to shrinkage*) x kL^2,
where, k is a constant depending on the pattern of loading.

3.2. Ultimate limit state

As discussed in Section 3.1, an allowable stress method of design is recommended for OPBF-RC. Therefore, consider a model cross-section as shown in Fig. 6.

Similar to reinforced concrete design, the following assumptions are made: (a) plane sections remain plain, (b) the contribution of concrete to tensile stresses is negligible, (c) the bond between reinforcement and concrete remains constant with time, and (d) member is prismatic. Let n be the modular ratio and A_T the area of OPBF-strand reinforcement, then:

$$\rho = \frac{A_T}{bd} \tag{14}$$

where b is the *breadth of the section*, ρ is the *reinforcement ratio* and A_T is the *area of OPBF reinforcement*. By transforming the area of reinforcement:

$$nA_T = n\rho bd \tag{15}$$

The compressive force in concrete (F_c) can be written as:

$$F_c = \frac{1}{2} f_c b\alpha d \tag{16}$$

where f_c is the compressive stress in concrete, b and d is the breadth and effective depth (respectively) of the cross-section, and α is the neutral axis depth factor. To determine the depth of the neutral axis ($x = \alpha d$), take the moment of areas about the designated arbitrary neutral axis (x) shown in Fig. 6:

$$b(\alpha d)\frac{\alpha d}{2} = n\rho bd(d - \alpha d) \tag{17}$$

Expanding Eq. 17 gives:

$$\alpha^2\frac{bd^2}{2} + \alpha\left(n\rho bd^2\right) - n\rho bd^2 = 0 \tag{18}$$

Dividing both sides of Eq. 18 by 'bd^2':

$$\alpha^2\frac{1}{2} + \alpha(n\rho) - n\rho = 0 \tag{19}$$

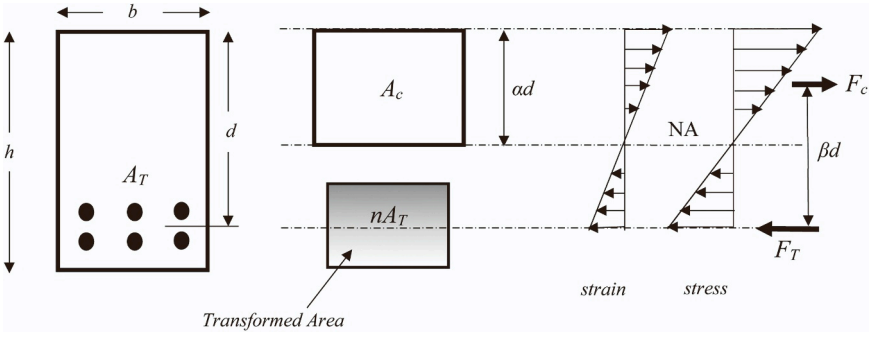

Fig. 6. Cross-section illustrating elastic stress and strain blocks of model OPBF-RC beam.

Solving α as the subject of Eq. 19 gives

$$\alpha = \sqrt{(np)^2 + 2np} - n\rho \tag{20}$$

Therefore, *depth of neutral axis* (x) would be

$$x = (\sqrt{(np)^2 + 2np} - n\rho)d \tag{21}$$

From Fig. 6, moment capacity due to OPBF-RC section can be determined by taking the moment of the force in strand reinforcement (M_T) about the centroid of the concrete in compression as:

$$M_T = F_T \beta d \tag{22}$$

where

$$\beta = 1 - \frac{\alpha}{3} \tag{23}$$

And the tensile stress in the strand reinforcement (f_T) can then be written as:

$$f_T = \frac{M_T}{A_T \beta d} \tag{24}$$

Also, from Fig. 6, the moment capacity due to concrete (Mc) above the neutral axis can be defined as:

$$M_c = F_c\, \beta d \tag{25}$$

Substituting for F_c from Eq. 16 into Eq. 25:

Table 1
Summary of allowable stress design examples 1, 2, and 3.

Design Example		1	2	3
Span (mm)		1300	4000	3500
Maximum design moment (kNm)		**26.7**	**103.0**	70.4
Preliminary sizing	$2.88\% \le \rho \le 10\%$	4.6	8.6	4.8
$1.5b \le h \le 3b$	b (mm)	200	230	230
	h (mm)	400	690	550
	d_e (mm)	320	530	450
Modular ration $= \frac{E_{opbf}}{E_{concrete}}$		0.813	0.839	0.926
Depth of neutral axis (mm) $x = d(\sqrt{(np)^2 + 2np} - n\rho)$		320	167.48	116
Lever arm (mm) $\beta = (1 - (\alpha/3)).d_e$		162.4		411.3
Stress in concrete (MPa) $< 0.45 f_{cu}$		12.90	11.32	12.83
Stress in OPBF strand < 165 MPa		37.55	20.67	34.23
Provided reinforcement (strand) area (mm^2)		**$6 \times 25\Phi_T$** **$A_{T,\,prov} = 2944$ mm^2**	**$15 \times 30\Phi_T$** **$A_{T,\,prov} = 10598$ mm^2**	**$6 \times 35\Phi_T$** **$A_{T,prov} = 5767$ mm^2**
Check spacing between strands > 25 mm		47.5		47.5
Provided nominal shear reinforcement (mm^2)		T8 @ 250 mm spacing $A_{sw} = 100$ mm^2	T8 @ 300 mm spacing $A_{sw} = 100$ mm^2	T8 @ 300 mm spacing $A_{sw} = 100$ mm^2
Calculate deflection $<$ span/250				
Curvature due to creep $\frac{1}{r_c} = \xi\left(\frac{1}{r}\right)_{cr} + (1-\xi)\left(\frac{1}{r}\right)_{uc}$		1.16×10^{-5} /mm	5.722×10^{-6} /mm	1.985×10^{-6} /mm
Curvature due to shrinkage $\frac{1}{r_{cs}} = \xi\left(\frac{1}{r}\right)_{cs(cr)} + (1-\xi)\left(\frac{1}{r}\right)_{cs(uc)}$		6.71×10^{-6} /mm	4.850×10^{-7} /mm	1.665×10^{-6} /mm
Total curvature $\frac{1}{r} = \left(\frac{1}{r}\right)_c + \left(\frac{1}{r}\right)_{cs}$		1.68×10^{-5} /mm	9.753×10^{-6} /mm	3.649×10^{-6} /mm
Deflection coefficient (k)		0.103	0.100	0.104
Midspan deflection (mm) $\delta_{max} = \frac{1}{r} kL^2$:		2.93 (< 5.2 OK)	15.61 (< 16 OK)	4.65 (<14 OK)

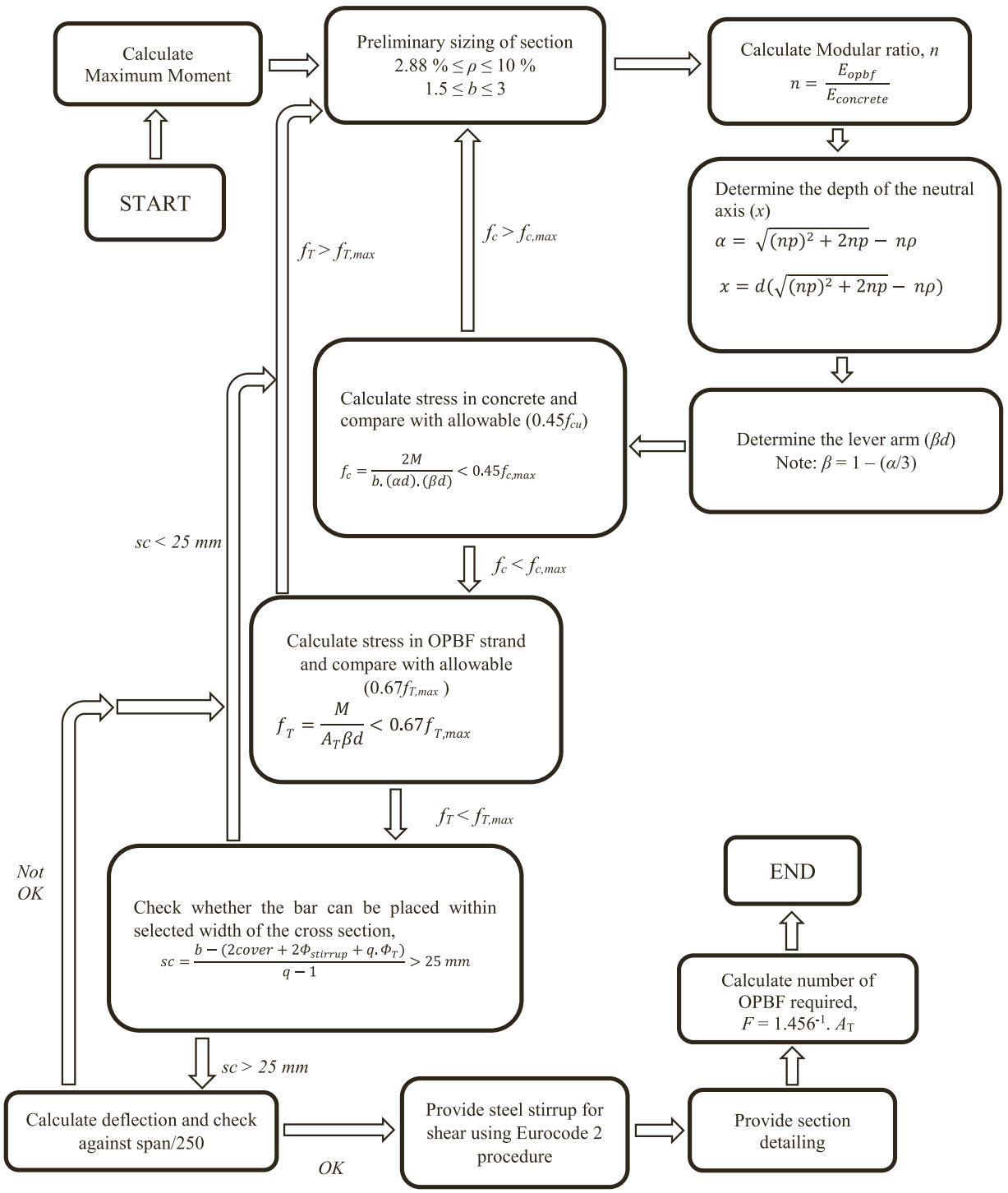

Fig. 7. Design flowchart for OPBF-RC beams.

$$M_c = \frac{1}{2} f_c b(\alpha d)(\beta d) \tag{26}$$

Similarly, compressive stress in the concrete (f_c) can be expressed as:

$$f_c = \frac{2M_c}{b(\alpha d)(\beta d)} \tag{27}$$

3.3. Design scenarios

From the allowable stress methodology and equations derived so far, the following calculations are possible:

- Determining the maximum moment to which the OPBF-RC beam will be subjected, and providing a section based on the calculated moment,
- Checking the adequacy of an already provided section and,
- Determining stress levels in OPBF strands.

A summary of the design procedure is presented in Section 3.4. Design examples have also been carried out to illustrate the 3 scenarios and are presented in Table 1, while the detailed calculations are contained in Appendix-2.

3.4. Design guidance summary

The following guide can be used for determining the moment capacity or calculating the adequacy of a section.

(i) Assume a reinforcement ratio in the following range $2.88\% \leq \rho \leq 10\%$. Recall Eq. 14 where $\rho = A_T/bd$. Detailing will become difficult beyond a reinforcement ratio of 10%). The following ratio is also recommended for determining the width (b) of the section: $1.5b \leq h \leq 3.2b$.
(ii) Determine Modular ratio $n = \frac{E_{opbf}}{E_{Concrete}}$, where E_{opbf} is the Young's modulus of the OPBF strands.
(iii) Determine the depth of the neutral axis ($x = \alpha d$) from Eq. 21.
(iv) Determine the lever arm (βd) from Eq. 23. Note that $\beta = 1 - (\alpha/3)$
(v) Calculate stress in concrete and compare with the allowable stress ($0.45f_{ck}$)
(vi) Calculate stress in OPBF strand and compare with the allowable stress ($0.67f_T$, where $f_T = 200$ MPa)
(vii) Check whether the bar can be placed within the selected width of the cross-section,

$$sc = \frac{b - \left(2cover + 2\Phi_{stirrup} + q\Phi_T\right)}{q - 1} \tag{28}$$

where b is the width of the section; $\Phi_{stirrup}$ is the diameter of the stirrup; q is the number of bars per layer of reinforcement; Φ_T is the diameter of OPBF-strand. It is recommended that sc > 25 mm. Eq. 28 is adapted from the ACI 361 code [53].
(viii) Calculate the number of single OPBF (F) required to obtain the reinforcement area (A_T) [36],
$F = 1.456^{-1}.A_T$;
where F is the number of single OPBF required for the calculated area of reinforcement A_T.
(ix) Provide nominal steel stirrup for shear.
(x) Calculate deflection and check against the Eurocode 2 limit of span/250.

The design guidance shown presented in Section 3.4 can be summarised into the flowchart presented in Fig. 7.

3.5. Design examples

3.5.1. Design scenario 1

Design an OPBF reinforced concrete rectangular lintel beam to resist the loading arrangement of Fig. 8. Characteristic strengths of concrete (f_c) and OPBF strand (f_T) are 40 MPa and 200 MPa respectively. *(Take $E_c = 32$ GPa and $E_{opbf} = 26$ GPa, use a material reduction*

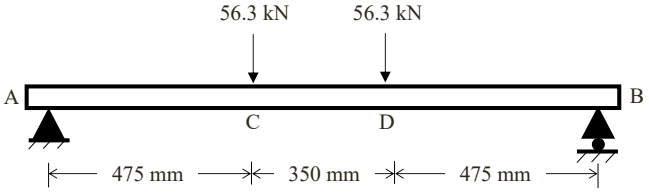

Fig. 8. Lintel beam showing loading arrangement.

factor (γ_m) of 1.5 for OPBF strand). Assume that construction props will be removed at 28 days.

3.5.2. Design scenario 2

A concrete lintel with an effective span of 4 m supports a 230 mm brick wall as shown in Fig. 9. The loads on the lintel are *Gk* = 100 kN and *Qk* = 40 kN. Determine suitable dimensions for the lintel if a 30 MPa concrete is used. *(Take* E_c = 31 GPa *and* E_{opbf} = 26 GPa*)*.

3.5.3. Design scenario 3

Design a simply supported OPBF-RC beam with span 3.5 m subjected to a uniformly distributed imposed load of 40 kN/m (Fig. 10). Assuming a beam dead load of 6 kN/m, and using the following allowable material strength, f_c = 13.5 MPa, f_T = 50 MPa, E_c = 27 GPa and E_{opbf} = 25 GPa. Design for the most critical section and determine the cracked moment capacity of the section after design.

A summary of the designs is presented Table 1, while the designed beam sections are shown in Figs. 11, 12 and 13 for design examples 1, 2 and 3, respectively with detailed calculations shown in Appendix-2. The OPBF-RC sections have also been compared with equivalents steel-RC sections.

Having carried out the design procedures, another area of practical concern for OPBF-RC would be aggregate sizing. Due to the low elastic modulus of OPBF strands, the area of reinforcement needed will be unusually high and concerns for compaction of concrete arises. It is therefore recommended that the maximum aggregate size is 10 mm to allow for proper compaction of concrete during placement. Consequently, the minimum spacing between bars should be greater than 25 mm or the bar diameter (whichever is the greatest). The minimum cover should not be less than the diameter of OPBF strands in order to adequately protect the strands. Other parameters to consider include the effect of the spacing of stirrups and the spacing of hose clamps on the flexural response of the full scale OPBF-RC beams.

Although experimental data is not yet available for full scale flexural elements of OPBF-RC, the finite element modelling procedure (i.e., concrete damage plasticity CDP) was used for the parametric study. The modelling was first validated using 100 × 100 x 500 mm OPBF-RC prisms.

4. Finite element modelling

4.1. Modelling of concrete

The concrete damage plasticity (CDP) concept, popular for modelling concrete, was used for the finite element (FE) modelling of the OPBF-RC and was implemented in Abaqus finite element software. The CDP concept requires the formulation of a single constitutive model incorporating both tensile and compressive failures, with appropriate values of the relevant parameters [54]. In other words, both compressive and tensile behaviour of concrete and OPBF strands need to be defined [55,56].

The modelling of compressive behaviour of concrete requires the definition of compressive stresses (f_c), and inelastic strains (ε^{in}). The experimental average compressive strength of 100 mm cubes of concrete together with the analytically derived strain at maximum compressive stress were used to derive the compressive stress – inelastic strain data that were imputed in the Abaqus software. For the analytical compressive strength data, the Ritter's parabola, with an ascending part defined by Eq. 29 and the descending part defined by Eq. 30, was used.

$$for\ 0 < \varepsilon < \varepsilon_o^{'}:\ \frac{f}{f_{cu}} = 2\frac{\varepsilon}{\varepsilon_o^{'}}\left(1 - \frac{\varepsilon}{2\varepsilon_o^{'}}\right) \tag{29}$$

$$for\ \varepsilon_o^{'} < \varepsilon < \varepsilon_{cu}:\ \frac{f}{f_{cu}} = 1 - 0.15\left(\frac{\varepsilon - \varepsilon_o^{'}}{\varepsilon_{cu} - \varepsilon_o^{'}}\right) \tag{30}$$

where f_{cu} is the maximum uniaxial compressive strength and ε is strain, ε_{cu} is the corresponding maximum strain defined by Eq. 31.

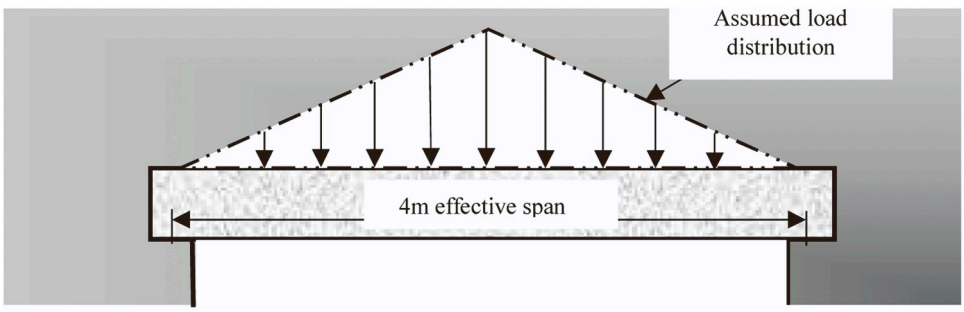

Fig. 9. Lintel beam showing assumed load distribution.

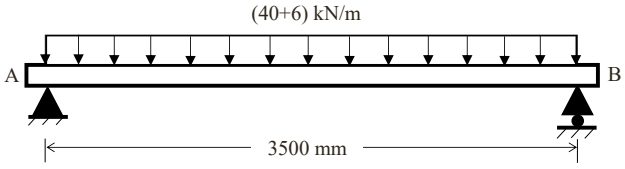

Fig. 10. Sketch of uniformly loaded simply supported beam.

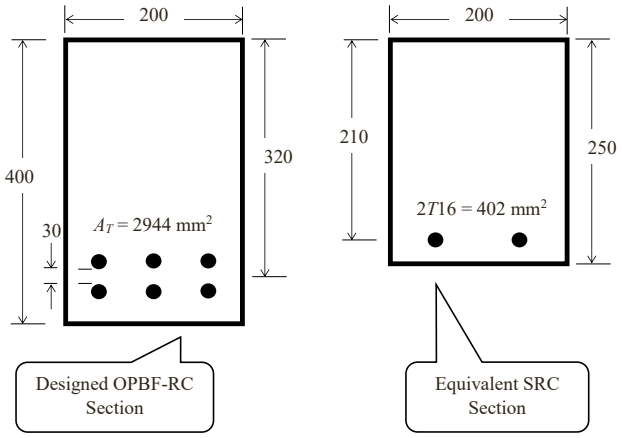

Fig. 11. Section provided for Example 1.

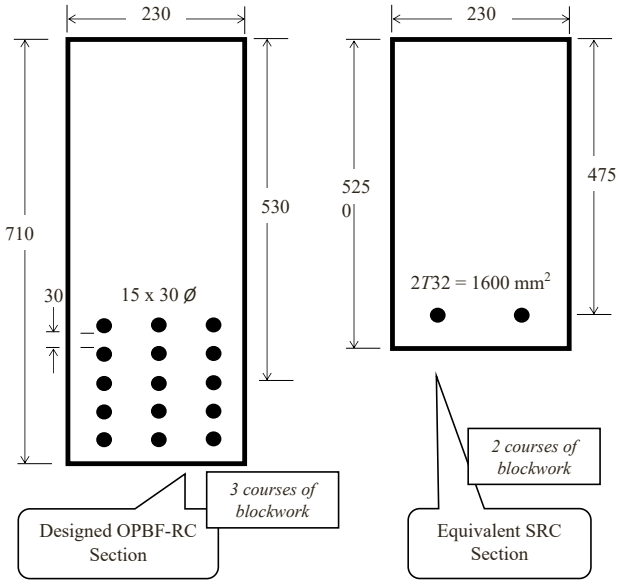

Fig. 12. Section provided for Example 2.

$$\varepsilon_o^{'} = (0.71 f_{cu} + 168) \text{ x } 10^{-5} \tag{31}$$

The yield stress was taken as 45% of the compressive strength (f_{cu}) derived from the compressive strength experiments [57–59]. In other words, the inelastic response of the concrete commenced at the yield stress as illustrated in Fig. 14 [36]. The total strain (ε_{cu}) is the sum of the elastic strain ε_o^{el} and the inelastic strain ε^{in} as defined in Eq. 32.

$$\varepsilon_{cu} = \varepsilon_o^{el} + \varepsilon^{in} \tag{32}$$

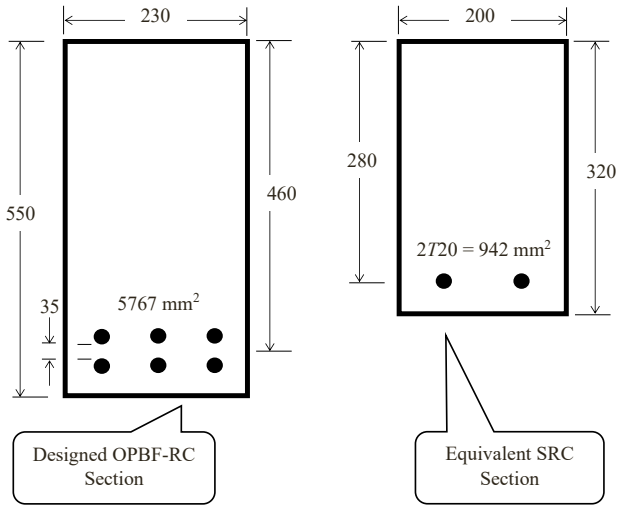

Fig. 13. Section provided for Example 3.

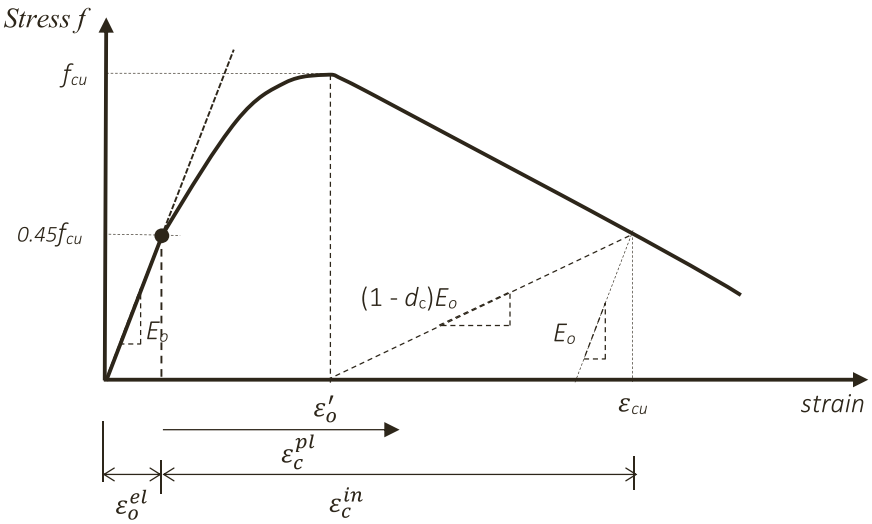

Fig. 14. Simplified analytical stress-strain curve for concrete under uniaxial compression.

where

$$\varepsilon_o^{el} = \frac{f_c}{E_0} \tag{33}$$

and E_o is the *Young's modulus* of the concrete.

The tensile behaviour of the concrete was modelled as a linear elastic ascending regime and an exponential decay regime (See Fig. 15) [58]. The exponential softening response was adopted such that:

$$for\ \ \varepsilon_t \le \varepsilon_{cr} : f_t = E_o \varepsilon_t \tag{34}$$

$$for\ \ \varepsilon_t \ge \varepsilon_{cr} : \frac{f_t}{f_{tu}} = \left(\frac{\varepsilon_{cr}}{\varepsilon_t}\right)^{0.4} \tag{35}$$

Where ε_t is the strain value along the tensile stress-strain curve and ε_{cr} is the cracking strain of the concrete [60]. The average maximum tensile strength (f_t) of 3.5 MPa from the experimental split-tensile strength test on 100 ϕ x 200 mm plain concrete cylinder samples, was used to generate the finite element tensile stress-strain data of the concrete.

Two (2) non-dimensional damage parameters (d_T) and (d_c), were defined to govern the tensile cracking and compressive crushing

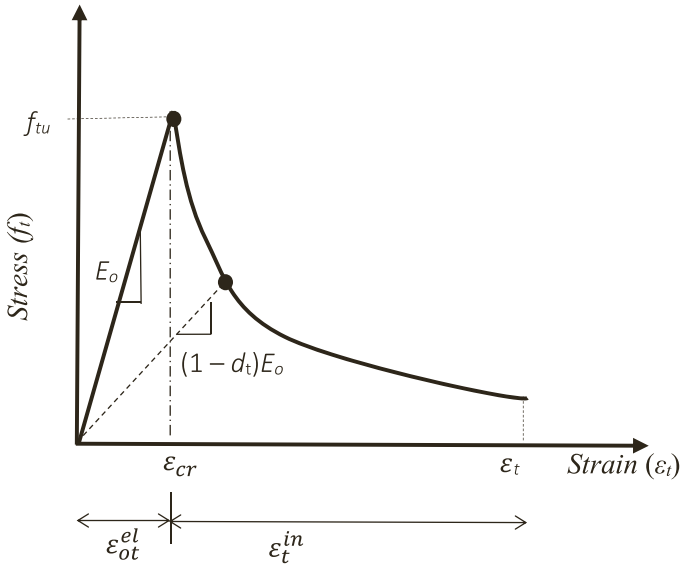

Fig. 15. Simplified analytical stress-strain curve for concrete under uniaxial compression.

of the concrete, respectively such that "$d = 0$" occurred in the elastic range and "$d = 1$" occurred at complete failure of the material. The damage parameters are defined in Eqs. 36 and 37.

$$d_t = 1 - \frac{f_t}{f_{tu}} \tag{36}$$

$$d_c = 1 - \frac{f_c}{f_{cu}} \tag{37}$$

where f_t and f_c are the tensile and compressive stresses, respectively, at any given point beyond the maximum stress f_{cu}. The damage curves employed for both concrete and OPBF strands are shown in Fig. 16.

In order to ensure a good degree of accuracy, the concrete was first modelled and calibrated against the compressive, tensile and flexural behaviour of the laboratory samples. The FE models with dimensions consistent with the experimental samples of 100 mm cubes, 100 ø x 200 mm cylinders and 100 x 100 x 500 mm prisms were discretized using 8-noded-brick elements with reduced integration (CD8R). The model parameters were then calibrated using through the Static, General (Full Newton) procedure in Abaqus. A comparison of the crack patterns as well as the stress-strain curves of the FE-models with the experimental curves show good agreement (see Fig. 17), thus indicating that accuracy of the selected CDP parameters. In Fig. 18, it can be observed that the post peak behaviour of the experimental curve does not match well with the numerical curve. But in fact, it is the experimental post-peak behaviour that is exaggerated due to the metal frame housing the LVDT device which prevented the sudden drop of the flexural stress after the cracking of the prism. The calibrated plain concrete models were then used to model the OPBF strands – reinforced concrete using quasi-static (dynamic, explicit) procedure [55]. The OPBF strands were similarly modelled using the CDP method with 8-noded-brick elements with reduced integration (CD8R). The stress-strain data for compression and tension for the concrete models

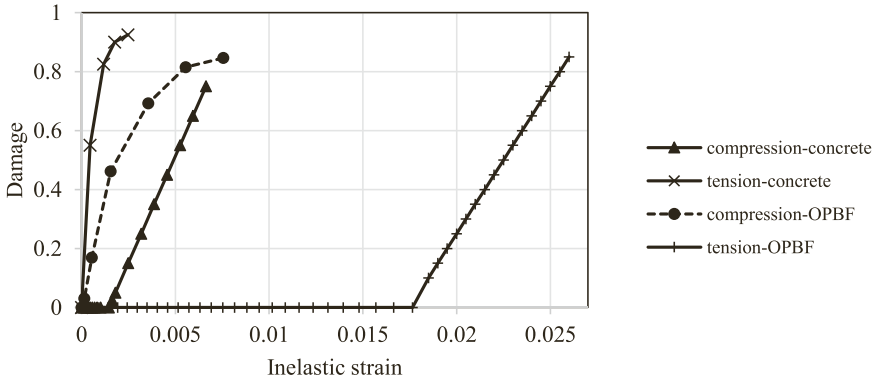

Fig. 16. Finite element damage curves of concrete and OPBF strands.

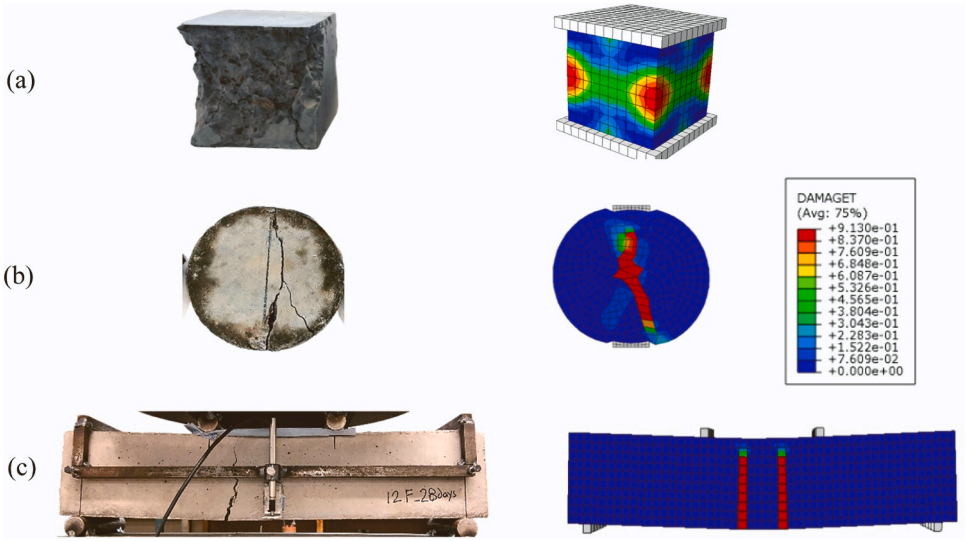

Fig. 17. Comparison of crack pattern of plain concrete FE-model with experimental sample (a) compressive strength (b) splitting tensile strength (c) flexural strength test.

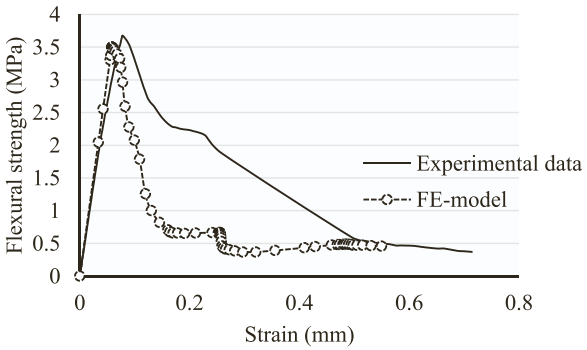

Fig. 18. Comparison between experimental and finite element flexural strength curves of 100 x 100 x 500 mm plain concrete prism.

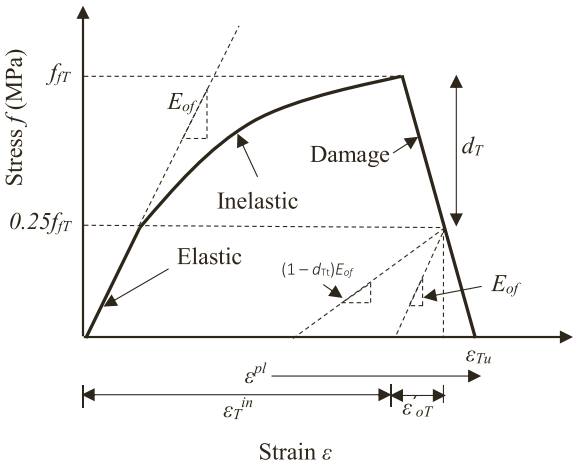

Fig. 19. Tensile streass-strain curve for clamp-enhanced OPBF strands.

used as inputs in Abaqus are presented in Appendix -1.

4.2. Modelling of OPBF strands

The use of the CDP approach for modelling tension reinforcement in concrete is very recent but provides good accuracy [36,61]. Similar to the CDP modelling of concrete, a simplified stress-strain relationship was observed from the tension and compressive test experiments of the OPBF strands (see Fig. 3) and this relationship was used to formulate the constitutive equations. From the tensile strength curves of the strands (in Fig. 3), the stress-strain relationship was characterised by three regimes: the ascending (elastic), the inelastic, and the linear damage regimes (also see Fig. 19), and are represented by Eqs. 38, 39 and 40, respectively [36].

$$for\ 0 < \varepsilon < \varepsilon_{oT}^{'} : f_f = E_{oT}\varepsilon \tag{38}$$

$$\varepsilon_{oT}^{'} < \varepsilon < \varepsilon_T : f_f = \alpha\varepsilon^2 + \beta\varepsilon + \gamma \tag{39}$$

$$\varepsilon_T < \varepsilon < \varepsilon_{Tu} : f_f = \lambda_1\varepsilon + \lambda_2 \tag{40}$$

Where f_{fT} is the maximum uniaxial tensile strength, ε_T is the corresponding strain and α, β, γ, λ_1 and λ_2 are constants. The inelastic strain ε_T^{in} is defined as the strain beyond which the strand changes from elastic response to inelastic response. The yield stress of the OPBF was determined as 25% of the maximum experimental tensile strength (f_{fT}) as shown in Fig. 3 (also see Fig. 19) while the total strain tensor ε_{Tf} is the sum of the elastic strain ε_{of}^{el} and the inelastic strain ε_f^{in} as defined in Eq. 41 [36].

$$\varepsilon_{Tf} = \varepsilon_{of}^{el} + \varepsilon_f^{in} \tag{41}$$

where

$$\varepsilon_{of}^{el} = \frac{f_f}{E_f} \tag{42}$$

and

$$E_f = (1 - d_{Tf})E_{oT} \tag{43}$$

where E_{oT} and E_f are the Young's modulus before and after the peak stress of the OPBF strands, respectively. Similar to the modelling approach for the concrete, a simplified relationship between stress at any given point (f_f) beyond the maximum stress (f_{fT} or f_{cT}) and a non-dimensional damage parameter for tension (d_{Tf}) and compression (d_{cf}) are defined as Eqs. 44 and 45, respectively [36].

$$d_{Tf} = 1 - \frac{f_f}{f_{fT}} \tag{44}$$

$$d_{cf} = 1 - \frac{f_f}{f_{cT}} \tag{45}$$

For the compressive behaviour modelling of the strands, the stress-strain relationship was simplified into two regimes: the elastic part and the descending/strain hardening decline (see Figs. 3 and 20) and defined by Eqs. 46 and 47.

$$for\ 0 < \varepsilon < \varepsilon_{oc}^{'} : f_{fc} = E_{of}\varepsilon \tag{46}$$

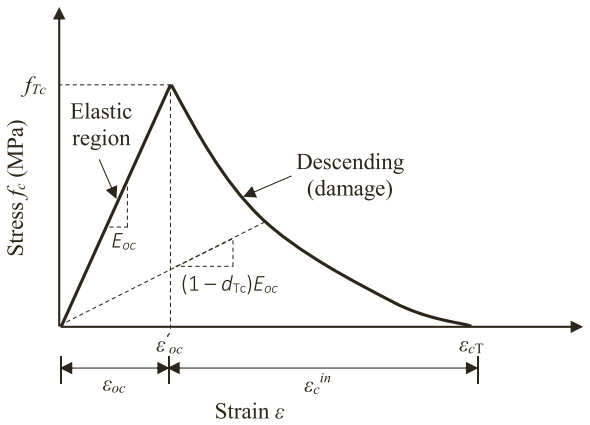

Fig. 20. Compressive stress-strain curve for clamp-enhanced OPBF strands.

$$\varepsilon_{oT}^{'} < \varepsilon < \varepsilon_{cT} : f_{fc} = \alpha_c \varepsilon^{\beta_c} \tag{47}$$

All the other parameters such as dilation angle (ψ), eccentricity (ε), the ratio of concrete strength in biaxial compression to uniaxial compressive strength (f_{b0}/f_{co}), and viscosity parameter, previously adopted for concrete modelling were used (see Table 2).

4.3. Modelling of bond between concrete and OPBF strand

The interfacial interaction between the strands and concrete was carried out through surface-based cohesive contact modelling [62]. This type of modelling is suitable for problems where the bond strength at the interface is relatively weak compared to the tensile and compressive strengths of the materials in contact [63] as well as where the thickness of the interface is negligible [64,65]. The modelling procedure assumes a traction-separation constitutive relationship and contact is defined as a surface interaction property rather than a material property, hence reducing computational efforts [66]. The linear post-damage softening of the strand-concrete interface was defined as a non-dimensional damage evolution criterion *D* which evolves from *0* to *1* beyond the peak bond stress (see Eq. 48) [67].

$$\sigma_i^D = (1 - D)\sigma_i^{'} \tag{48}$$

Where, σ_i^D is the contact stress after damage initiation and $\sigma_i^{'}$ is the contact traction at normal and shear directions (i).

The OPBF strands were assumed to be circular in cross-section while the hose clamps were modelled using C3D8R elements as rings with rectangular projection. A perfectly plastic mild steel with a yield strength of 350 MPa and a modulus of elasticity of 200 GPa was adopted for the clamps. To avoid surface penetration between the strands and concrete, "hard contact" was defined in the normal direction. The concrete beams were modelled with holes having diameter the same as that of the strands. The strands were then inserted to an embedment length of 80 mm just as in the experiments. While the relative motion at the concrete-OPBF interface was chosen as "small sliding" [40], the clamps were constrained as "embedded region" within the concrete. To simulate the pull-out of the strands, "encastre" boundary condition was applied over the concrete while a displacement of 25 mm was applied onto the free end of the strand. Fig. 21 (a) show the bond pull-out samples after the experiments, Fig. 20 (b) illustrates the clamp and bond pull-out FE model, and Fig. 20 (c) compares the simplified bond pull-out model with the experimental bond pull-out of 6 samples.

After the calibration of the bond model, a 100 x 100 x 500 mm OPBF-RC prism with a reinforcement ratio of 3.49 and with the strand hose clamp spaced at 45 mm c/c was modelled (see Fig. 22). Fig. 22 further shows that there is good agreement between the mechanical behaviour of the experimental model and that of the simulations. After this calibration of the mechanical properties of the concrete and OPBF strand models as well as the interfacial bond interaction, the parametric study was carried out.

4.4. Parametric studies

The parametric study was carried out to investigate the effect of clamp spacing, and stirrup spacing on the flexural capacity and failure mode of a 150 x 220 x 1300 mm concrete beam model reinforced with the OPBF strands. Fig. 23 presents details of the strand reinforcements and dimensions. From the experimental study, 3.49% of OPBF reinforcement ratio is equivalent to 0.56% steel reinforcement in terms of maximum flexural strength. By direct proportion, a 150 x 220 mm singly reinforced SRC section with 2-Ø14 mm bars (0.93% reinforcement ratio) would translate to the same section reinforced with 6-Ø20 mm OPBF strand reinforcement (5.71 reinforcement ratio) as shown in Fig. 23. For the steel reinforced model, tie constraint was defined between the reinforcement bars and concrete which assumes that there is no slip between concrete and the reinforcement, while a cohesive surface, consistent with the FE bond modelling in Section 4.3, was defined for the concrete-OPBF interface. A stirrup spacing of 200 mm centre-to-centre was adopted for the steel reinforced section. Fig. 24 presents the flexural response of the SRC beam model and that of an equivalent OPBF-RC model.

While the moment at first crack for the SRC beam model is 14.64 kNm, the first crack for the OPBF-RC beam model occurs at 9.79 kNm. The early cracking in the OPBF-RC model is due to the lower modulus of elasticity of the reinforcement, thereby making the concrete the stiffer path for load transfer. The onset of cracking redirects the load path to the OPBF reinforcement, thereby increasing the moment capacity of the section. The moment-deflection curve of the SRC beam model is however steeper than that of the OPBF-RC model due to the higher Young's modulus of the steel reinforcement and better bonding between the steel bars and concrete. At the

Table 2
Material properties and CDP parameters of concrete and OPBF strands.

Property	Concrete	OPBF strands	Reference
Density (kg/m^3)	2340	840	This study
Young's Modulus E (GPa)	32.2	26.6	This study
Poisson ratio	0.15	0.4	This study
Dilation angle ψ	35^0	35^0	[36]
Eccentricity €	0.1	0.1	[36]
f_{bo}/f_{co}	1.16	1.16	[36]
K	0.67	0.67	[36]
Viscosity Parameter	0	0	[36]

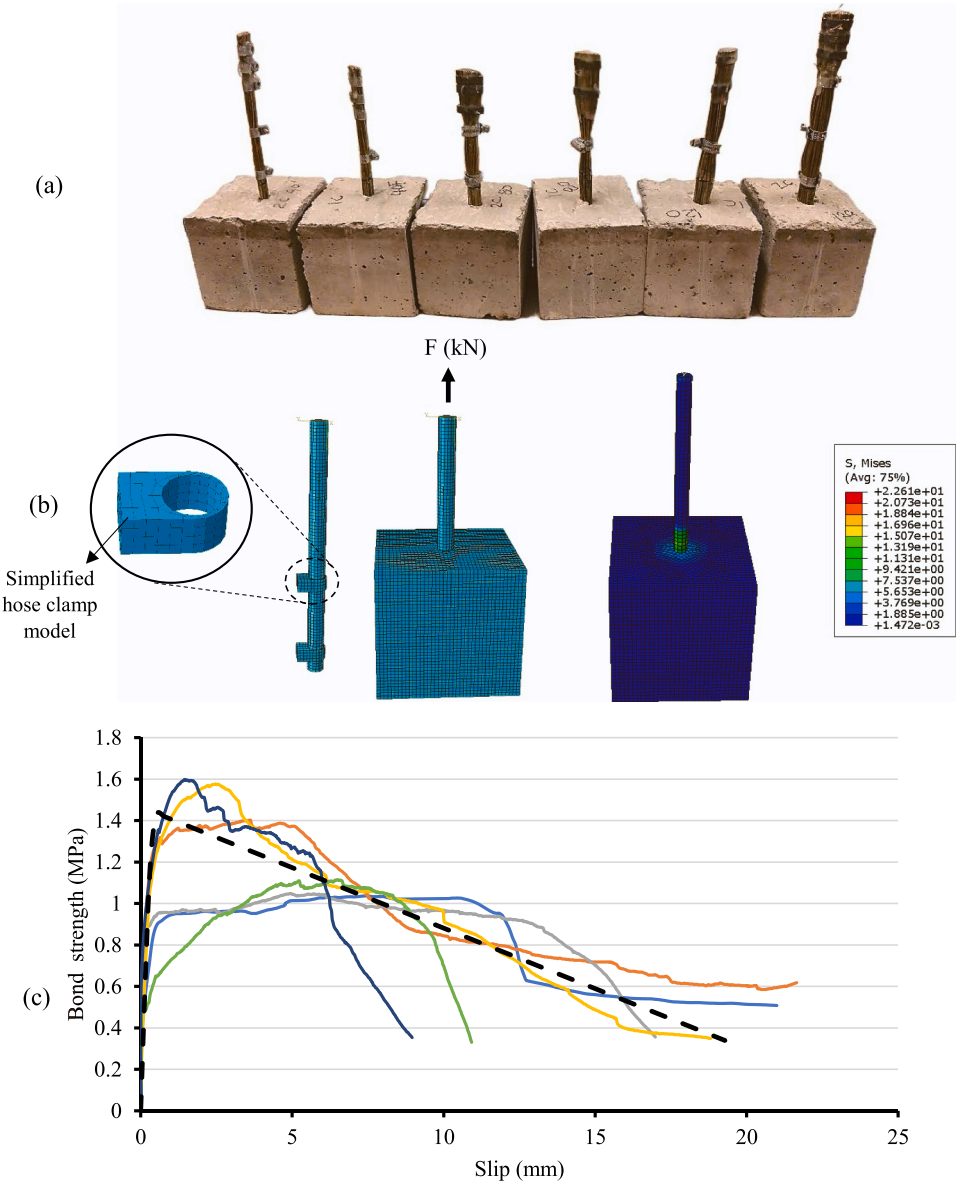

Fig. 21. (a) Samples after bond pull-out experiment (b) Bond-pull-out model (c) Bond pull-outs curves from experiments (continuous lines) and finite element bond pull-out curves (bilinear broken line).

deflection limits of span/500 to span/250 specified by Eurocode 2, the moment capacity of the OPBF-RC model is only about 70% (32.48 kNm) of that of the SRC model (45.05 kNm). Although the ultimate moment capacities of both models are comparable, the OPBF-RC would undergo about thrice more deflection to achieve this maximum moment capacity, which is similar to the flexural response of the 100 x 100 x 500 mm prism specimen from experiments (see Fig. 4).

The effects of parameters such as stirrup spacing, and clamp spacing on the crack pattern and flexural response of OPBF-RC were also investigated using the developed FE-model. Fig. 25 shows that the effect of stirrup spacing on the flexural performance of the OPBF-RC model is negligible. The model without stirrups shows a lower moment capacity after 2 mm of midspan deflection. The crack paths (Fig. 26) show a predominant bending (flexural) crack pattern gradually evolving into major shear cracks as the stirrup spacing is increased from 100 mm to 300 mm. For the 300 mm spacing, more shear cracks appear and travel from the bottom to the top of the section without being bridged by stirrup action. For the model without stirrups, no resistance to shear cracks is provided and hence, the beam fails in a predominantly shear mode. Fig. 27 shows that with an increase in the clamp spacing, the flexural capacity of the OPBF-RC is reduced. The reduction in flexural capacity is due to a reduced stress transfer between the OPBF strands and the concrete. Without clamps, the bonding between the strands and concrete would be poor and failure will be sudden with a few large cracks as revealed in Fig. 28. Hence a maximum clamp spacing of 350 mm is recommended.

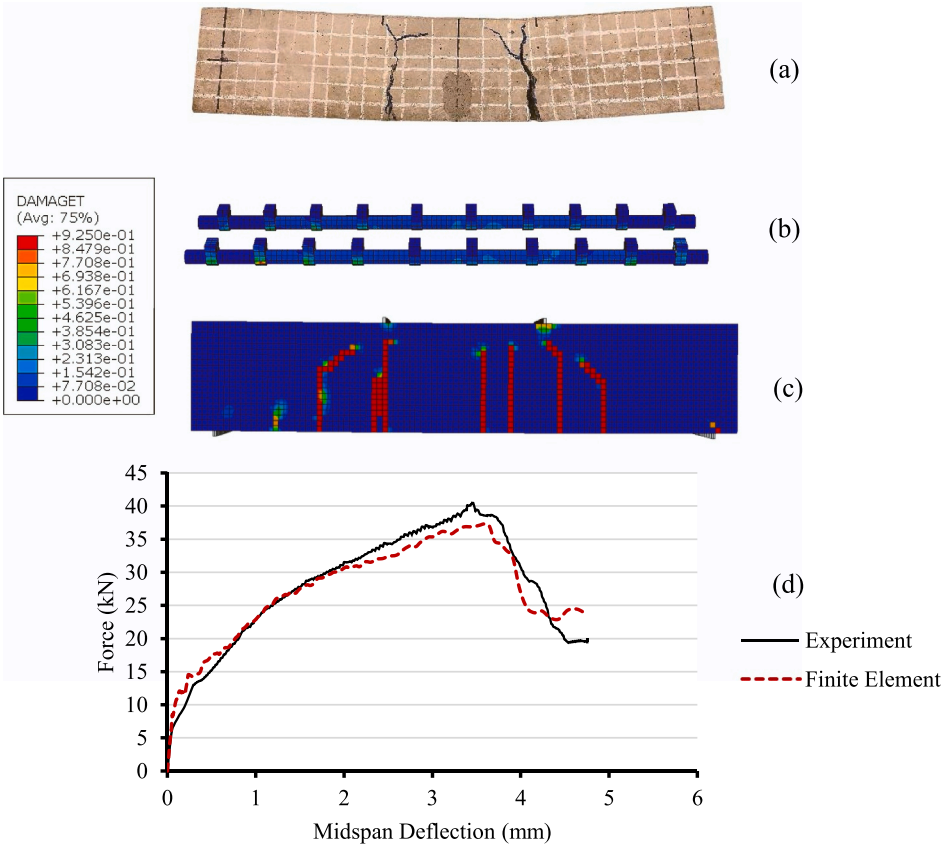

Fig. 22. (a) Concrete prism after 4-point flexural strength test (b) Clamp-enhanced OPBF strand reinforcement (c) Finite element model of concrete prism showing crack pattern (d) Comparison between experimental and finite element flexural strength behaviour.

4.4.1. Effect of stirrup spacing on flexure

The design for shear as shown in Table 1 implies that shear is not critical for OPBF-RC beams. This is due to the relatively low modulus of elasticity of the OPBF strands. The FE results also show no benefit of employing stirrup spacing of less than 300 mm under service loads. However, at the ultimate flexural capacity of the beam, crack patterns transit from predominantly bending cracks (for 100 mm stirrup spacing) to shear cracks (for the 300 mm stirrup spacing). No improvement was observed in ultimate flexural strength with or without stirrup although improvement in shear crack control due to the presence of stirrups can be noticed (see Figs. 26 and 27).

4.4.2. Effect of clamp spacing on flexure

Without hose clamps, there would be unrestricted slip between adjacent fibres making up the strands. The procedure used in the study of Momoh et al. [40], although improved bond strength, may not provide a rigid system of reinforcement for a load-bearing structural element. The flexural response in Fig. 28 indicates that hose clamps spacing should be limited to 350 mm. The natural length of OPBF, which is between 500 mm and 1200 mm [39], also implies that a clamp spacing greater than 350 mm may restrict the use of shorter fibre strands. Hence a clamp spacing of 350 mm is recommended for OPBF-RC beams.

5. Economic and environmental considerations

5.1. Economic comparison

A comparison between the OPBF-RC and equivalent SRC beams as shown in design examples 1, 2 and 3 was carried out in terms of actual monetary costs of the beams and the amount of carbon dioxide emission to the environment. The beams are assumed to have been constructed in rural North Central Nigeria where the average cost of a cubic metre of concrete is about £ 52.58, and a hose clamp is £ 0.018. It is assumed that OPBF is sourced for free from oil palm waste biomass. Table 3 provides a summary of the quantities and cost calculations. Although there was about 35% average reduction in the volume of concrete for the OPBF-RC, some of the savings in

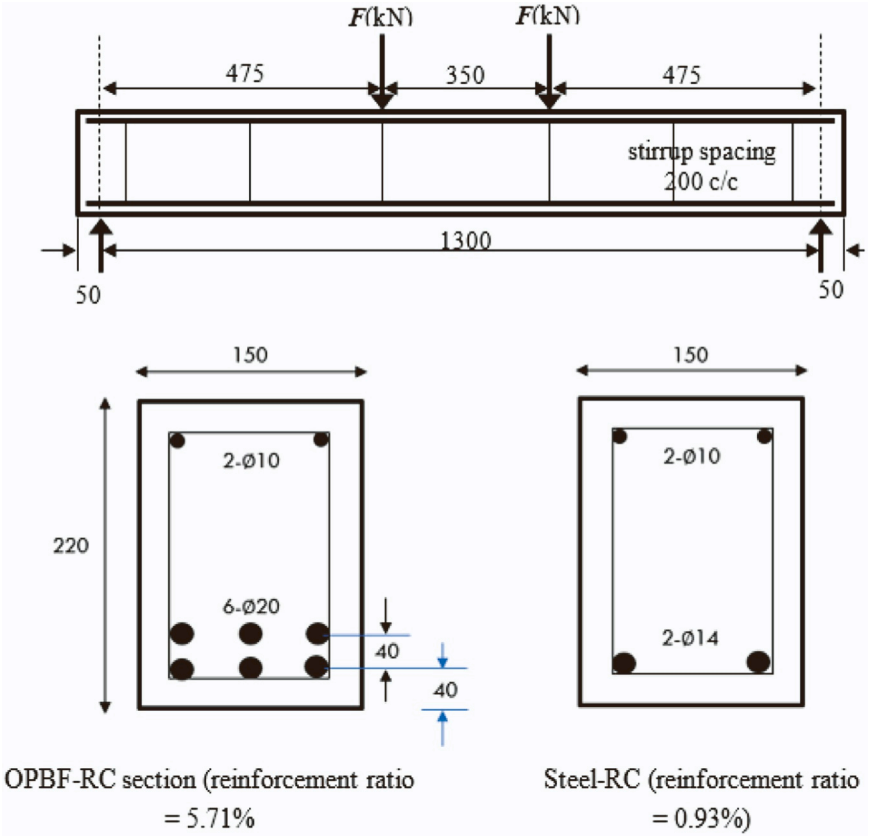

Fig. 23. Beam details used for the parametric study.

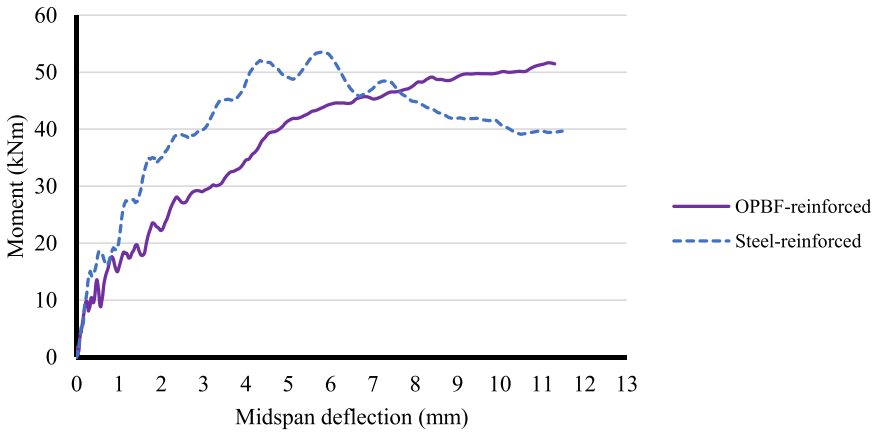

Fig. 24. Comparison between OPBF-RC beam FE-model and SRC FE-model.

cost were negated by the use of hose clamps. But over 10% cost in savings can still be achieved. A more economic design can be achieved for the OPBF-reinforced concrete beam in design example 3 by reducing the concrete section.

5.2. Short-term carbon footprint assessment

The comparison between the OPBF-RC and equivalent SRC beam sections as shown in design examples 1, 2 and 3 in terms of carbon dioxide emissions was divided into two sections: Carbon dioxide emission associated with (1) material manufacture, and (2) material transportation.

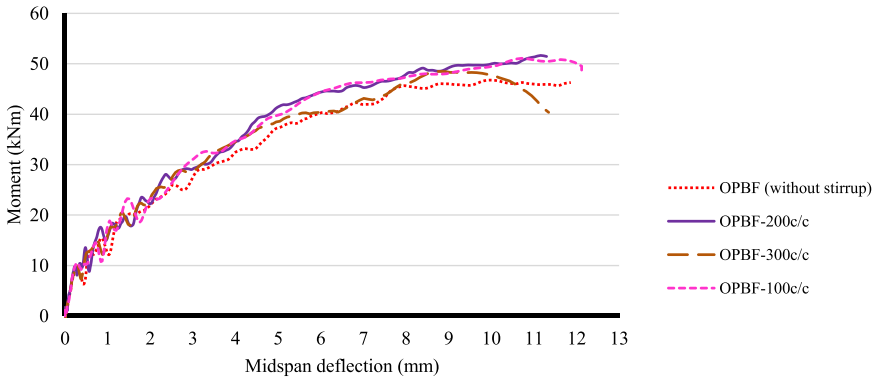

Fig. 25. Effect of stirrup spacing on flexural performance of OPBF-RC beams.

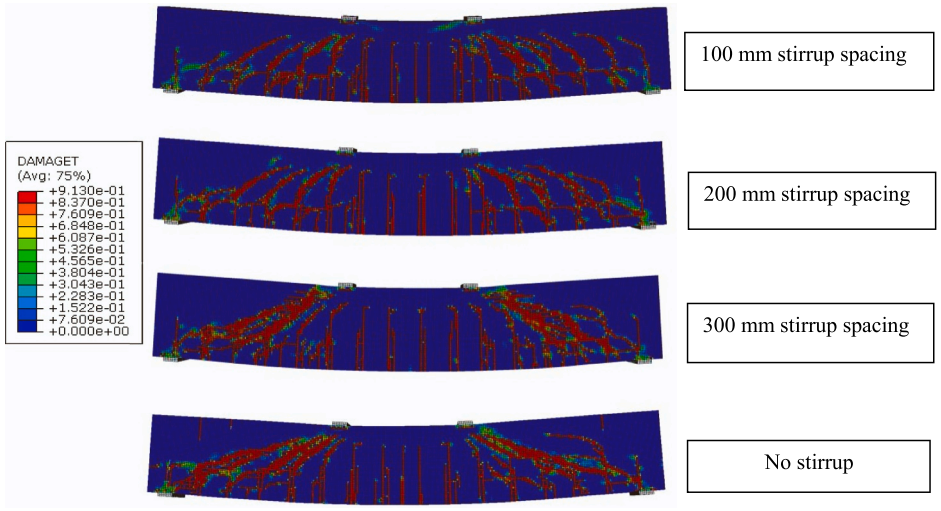

Fig. 26. Effect of stirrup spacing on crack patterns of OPBF-RC beams.

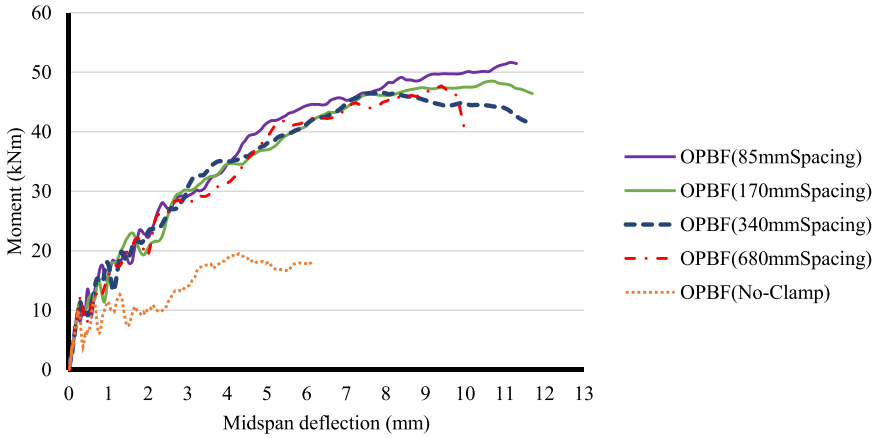

Fig. 27. Effect of hose clamp spacing on flexural response of OPBF-RC beams.

5.2.1. CO_2 due to material manufacture

Carbon emissions from the production of concrete, steel and OPBF were assumed as 173 $kgCO_2/m^3$ [68], 1.9 $kgCO_2/kg$ [69] and 0.0 $kgCO_2/m^3$ respectively. Using the quantities calculated in Table 3 for design examples 1, 2 and 3, the quantities of CO_2 emission

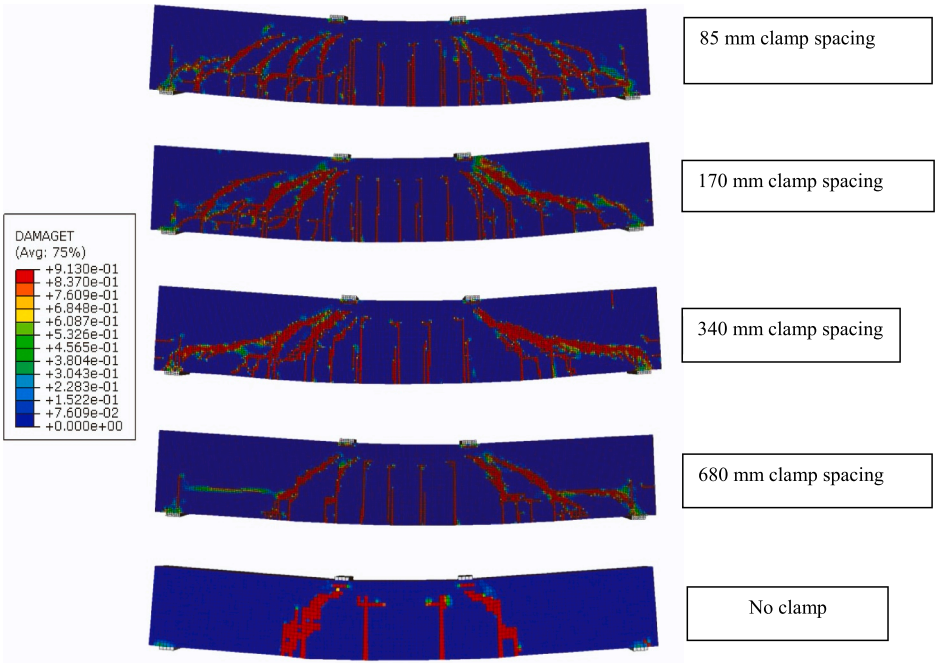

Fig. 28. Effect of hose clamp spacing on crack patterns of OPBF-RC beams.

Table 3
Summary of quantities and cost calculations from design examples.

Design Example	Volume of concrete in m^3 (Cost of concrete in £)		% Difference in concrete volume	Cost of reinforcement (£)		Total cost (£)		% savings
	OPBF strand RC	Equivalent Steel RC		OPBF strand RC	Equivalent SRC	OPBF RC	Steel RC	
1	0.1002(5.27)	0.0645(3.39)	35.6	0.018x24 = **0.43**	2.97	5.7	6.36	11.6
2	0.6108(33.12)	0.4766(25.06)	22.0	0.018x180 = **3.24**	18.29	36.36	43.35	16.1
3	0.4226(22.22)	0.2218(11.66)	47.5	0.018x60 = **1.08**	9.09	23.3	20.75	-2.6

Table 4
Summary of the material quantities and corresponding carbon dioxide emissions.

Design Example	Volume of concrete in m^3 (CO_2 emission in kg) [A]		% difference in CO_2 emission (from concrete)	CO_2 emission in kg [B]		% difference in CO_2 emission (from Steel)	CO_2 Emissions from materials (kg) [A] + [B]	
	OPBF strand RC	Equivalent Steel RC		Steel clamps for OPBF in OPBF-RC beam	Steel rebar in SRC beam		OPBF-RC beam	Equivalent SRC beam
1	0.1002 (17.340)	0.0645 (11.161)	+ 35.6	1.368	7.458	-81.7	18.708	18.62
2	0.6108 (105.67)	0.4766 (82.470)	+ 22.0	10.260	94.560	-84.3	115.93	177.93
3	0.4226 (73.127)	0.2218 (38.380)	+ 47.5	3.420	32.813	-89.6	76.55	71.19

Weight of materials in kg are shown without brackets, while brackets indicate the corresponding CO_2 emissions in grams

were calculated for concrete, steel and OPBF by multiplying the volume of the three materials with their respective unit CO_2 emissions. The second column of Table 4 is split into 2 sub-columns: the first and second sub-columns present the volume of concrete for OPBF-RC beam and an equivalent SRC beam, respectively, with each calculated CO_2 emission in bracket. The third column shows the percentage differences between the CO_2 emission due to the respective volumes of concrete in the OPBF-RC and SRC beams. As a result of the concrete sections required for the OPBF-RC beams, the percentage CO_2 emission due to concrete is greater than that of equivalent SRC beams by about of 22 – 48%. The fourth column of Table 4 is further divided into 2 sub columns: the first and second sub-columns show the CO_2 emissions for the steel clamps used to hold single OPBF together into strands (in the OPBF-RC beam), and the reinforcing steel

in the SRC beam, respectively. The fifth column shows the percentage differences between the CO_2 emission due to the respective weights of steel used in the OPBF-RC and SRC beams. The last column is the CO_2 emission for the beams; divided into two sub-columns: the first and second sub-columns show the total CO_2 emissions for the steel clamps in the OPBF-RC beam, and the reinforcing steel in the SRC beam, respectively. The CO_2 emissions from each beam type were obtained by adding CO_2 emissions ([A] + [B]), due to the respective volumes of concrete [A] and weights of steel [B] in the second and fourth columns of Table 4. It was observed that in terms of CO_2 emission during the production of either beam type, there is no marked difference as the savings in due to the elimination of steel in the OPBF-RC were negated by the relatively higher concrete volume.

5.2.2. CO_2 due to material transportation

To calculate the CO_2 emissions resulting from road transportation of the materials, it was assumed that the distance from the point of purchase/source to the construction site is 5 km. Taking the density of steel as 7850 kg/m^3 and that of OPBF as 840 kg/m^3, transporting a unit volume of each material would mean transporting either 7850 kg of steel or 840 kg of OPBF. To transport 7850 kg of steel, 4 trips of a light duty vehicle (LDV) (which is representative of vans used in the geographical area under consideration) with a 2000 kg payload capacity [70] would be needed. Then we multiply *mass* x *distance* (i.e., 7850 kg x 5 km) which gives 39250 kg-km. The LDV needs to make 3 return (unladen) trips, for which it was assumed that the LDV transports only 1 kg of load each for the 3 return trips, (i.e., 1 kg x 5 km x 3 trips) thereby resulting in 15 kg-km. The total carbon dioxide emission for transporting 7850 kg of steel is therefore 39265 kg-km. Similarly, to transport 840 kg of OPBF, a single trip on an LDV would be adequate. If we multiply *mass* and *distance* (i.e., 840 kg x 5 km) we get 4200 kg-km.

Average weight-based CO_2 emission factor for an LDV is 7.454×10^{-4} kgCO_2/(kg-km) [70]. Therefore, the amount of CO_2 emission for transporting the steel would be 39265 kg-km multiplied by 0.0007454 kg CO_2/kg-km which is 29.268 kgCO_2 (for the 7850 kg of steel). Therefore, the CO_2 emission rate for the steel is 29.268 kgCO_2 divided by 7850 kg which is 3.728 x 10^{-3} kgCO_2/kg. Similarly, the amount of CO_2 emission in transporting the 840 kg of OPBF would be 4200 kg-km multiplied by 0.0007454 kgCO_2/kg-km which is 3.131 kgCO_2. The CO_2 emission rate for the OPBF is therefore 3.131 kgCO_2 divided by 840 kg which is 3.727 x 10^{-3} kgCO_2/kg. Recall that the OPBF reinforcement in the OPBF-RC beam is composed of the steel hose-clamps and the OPBF strands themselves as shown in Table 5. The second column of Table 5 shows the total weight of steel hose clamps while the corresponding CO_2 emissions are shown in brackets calculated by multiplying the CO_2 emission rate for the steel (i.e., 3.728 x 10^{-3} kgCO_2/kg) with the total weight of the steel hose clamps. The second column of Table 5 presents the total weight of OPBF strands while the corresponding CO_2 emission is shown in brackets for each design example. Similarly, the CO_2 emissions in bracket were calculated by multiplying the CO_2 emission rate for OPBF (i.e., 3.727 x 10^{-3} kgCO_2/kg) with the total weight of steel hose clamps. From the summary of Table 5, there seem to be no advantage from using OPBF instead of steel reinforcement with regards to the amount of CO_2 emissions for design example 3 due to the relative over-design of the OPBF-RC beam. Nonetheless, if the importation of steel is considered, the savings in CO_2 would be significant even for design example 3. From design examples 1 and 2, carbon dioxide emissions can be reduced by up to 30%.

Although a basic comparison in terms of economic and environmental implications between OPBF-RC and SRC beam sections has been presented, other factors such as differences in labour cost, the introduction and acceptability of the new technology, and onsite techniques have not been captured and are areas for further study. For most developing countries in sub-Saharan Africa, OPBF is locally sourced where-as steel is imported. This importation involves transoceanic transportation with attendant CO_2 emissions which have not been considered in this study. Hence it is evident that the use of OPBF reinforcement will be beneficial to the environment.

Compared to a conventional construction material like steel, OPBF is derived from oil palm tree, making it an abundant and renewable resource. This can be a significant advantage in terms of savings in cost and CO_2 emissions, in countries where oil palm cultivation generates substantial biomass waste. From this study, the 30% savings in CO_2 emissions through the use of OPBF strand is equivalent to about 500 kg of CO_2 emission for manufacturing 1 tonne of steel [71], not to mention CO_2 savings by avoiding transportation or importation of steel. Furthermore, the continuous use of conventional construction materials has been projected to claim between 35–60% of the remaining carbon budget associated with limiting the global temperature increase to below 2 °C by the year

Table 5
Summary of carbon dioxide emissions for each design example.

Design Example	Weight of material in *kg* (CO_2 emission in transportation in *g*)				% difference in CO_2 emission
	OPBF-RC beam			SRC beam	
	Hose clamps [A]	OPBF Strands [B]	CO_2 emission for OPBF strands [A] + [B]	Steel Rebars	
1	0.72 (2.684)	3.21 (11.964)	(14.648)	5.22 (19.462)	**24.9**
2	5.40 (20.133)	35.61 (132.732)	(152.865)	64.31 (239.774)	**36.2**
3	1.80 (6.711)	16.96 (63.216)	(69.927)	17.25 (64.315)	**- 8.7**

Weight of materials in kg are shown without brackets, while brackets indicate the corresponding CO_2 emissions in grams

2100 [72]. Nevertheless, further studies are required in order to encourage uptake of innovations like OPBF-RC. For instance, the degradation of the bond strength of OPBF with concrete over time due to alkali-induced surface degradation, require further investigation. The relatively low elastic modulus of OPBF strands compared to steel creates localised cracks and increased deflection. This characteristic may limit its application with high structural demands. Therefore, fibre pre-treatment methods such as coatings, together with additional measures like using hose clamps are necessary to mitigate bond degradation, prevent slippage between fibres and enhance monolithic action. The variations in flexural behaviour of the OPBF-RC under different temperatures, humidity and different loading scenarios is scheduled for further investigation. This study recommends OPBF-RC for lightly loaded beams or structures with less demanding structural requirements like lintels. In summary, while OPBF shows promise as a sustainable and potentially low-cost construction material, its effective use requires addressing challenges related to bond strength, interface degradation, and bespoke design methodology as described in this paper.

6. Conclusions

This paper focused on the design procedure for OPBF strand reinforced concrete beams. The design philosophy for conventional steel reinforced concrete beams was briefly discussed in relation to the elastic modulus of OPBF strands and the bond behaviour between concrete and the strands. Design examples were presented and the economic and environmental impact of using the strands as reinforcement was compared to using conventional steel reinforcement rebars. Consequently, the following key findings are highlighted:

- The relatively low elastic modulus of the OPBF strands and the low bond strength between the strands and concrete necessitates a different research approach. Hence the Allowable Stress design method is recommended.
- A hybrid concrete beam having OPBF strands as longitudinal reinforcement and steel stirrup as shear links is adopted. The steel stirrups are meant to resist shear cracks.
- Due to the relatively low elastic modulus of the OPBF strands, shear failure is not critical, hence nominal shear links may be provided.
- Deflection of OPBF reinforced beams should be calculated from the effects of loading on the beam's curvature with respect to creep and shrinkage. The calculated deflection can then be checked against the span/500 to span/250 limit provided by Eurocode 2.
- Up to 16% and 36% savings in cost and carbon dioxide emissions, respectively, can be achieved by using an OPBF reinforced lintel instead of a conventional steel reinforced lintel. Savings in CO_2 would be more if carbon emissions resulting from trans-oceanic transportation of steel is considered for countries that import steel.
- A viable method of splicing the OPBF strands should be investigated.
- Concrete damage plasticity (CDP) concept of finite element modelling provides a simplified procedure for modelling OPBF strand reinforced concrete.
- This study assumed that the bond strength between the OPBF reinforcement strands and concrete remains constant. Further analysis is required to incorporate possible age-induced bond reduction at the strand-concrete interface.

Declaration of generative (AI) and AI-assisted technologies in the writing process

The authors did not use any generative AI and AI-assisted technology in the writing of this paper.

CRediT authorship contribution statement

Momoh Emmanuel Owoichoechi: Conceptualization, Data curation, Formal analysis, Funding acquisition, Investigation, Methodology, Resources, Software, Visualization, Writing – original draft, Writing – review & editing. **Osofero Adelaja Israel:** Conceptualization, Funding acquisition, Methodology, Project administration, Supervision, Writing – review & editing. **Menshykov Oleksandr:** Investigation, Supervision, Writing – review & editing.

Declaration of Competing Interest

The authors declare that they have no known competing financial interests or personal relationships that could have appeared to influence the work reported in this paper.

Data availability

Data will be made available on request.

Acknowledgement

This research was sponsored by the overseas PhD scholarship scheme of the Nigerian Petroleum Technology Development Fund (PTDF). The authors also wish to thank the University of Exeter for providing the open access fund to cover the publication cost of this research.

Appendix-1. Stress-strain data used in Abaqus

A.1.1. Stress-strain data in compression and tension of concrete used in the finite-element modelling

Compression			Tension		
Compressive stress f_c (MPa)	Inelastic strain ε^{in}	Damage parameter d_c	Tensile stress f_c (MPa)	Inelastic strain ε_t^{in}	Damage parameter d_t
18	0	0	3.45	0	0
22	0.00013905	0	1.8	0.000456	0.478
26	0.000294623	0	0.7	0.001181	0.797
28	0.000380814	0	0.4	0.001762	0.884
30	0.000474542	0	0.3	0.002477	0.913
32	0.000578215	0			
34	0.000695889	0			
36	0.000835469	0			
38	0.001017379	0			
40	0.00145654	0			
39	0.001629207	0.025			
38	0.001801874	0.05			
34	0.00249254	0.15			
30	0.003183207	0.25			
26	0.003873874	0.35			
22	0.004564549	0.45			
18	0.005255216	0.55			
14	0.005945874	0.65			
10	0.00663654	0.75			

A.1.2. Stress-strain data in compression and tension of OPBF strands used in the finite element modelling.

Tension			Compression		
Stress MPa	**Inelastic strain**	**Damage**	**Stress MPa**	**Inelastic strain**	**Damage**
65	0	0	65	0	0
70	0.000433	0	50	0.000188	0.230769
75	0.000924	0	40	0.000752	0.384615
80	0.001422	0	30	0.001881	0.538462
85	0.001928	0	20	0.003573	0.692308
90	0.002442	0	10	0.01072	0.846154
95	0.002966	0			
100	0.003498	0			
105	0.004041	0			
110	0.004593	0			
115	0.005157	0			
120	0.005733	0			
125	0.00632	0			
130	0.006922	0			
135	0.007537	0			
140	0.008168	0			
145	0.008815	0			
150	0.00948	0			
155	0.010164	0			
160	0.01087	0			
165	0.011599	0			
170	0.012354	0			
175	0.013137	0			
180	0.013953	0			
185	0.014805	0			
190	0.0157	0			
195	0.016644	0			
200	0.017645	0			
180	0.0185	0.1			
170	0.019	0.15			
160	0.0195	0.2			
150	0.02	0.25			
140	0.0205	0.3			
130	0.021	0.35			

(*continued on next page*)

(*continued*)

Tension		Compression
120	0.0215	0.4
110	0.022	0.45
100	0.0225	0.5
90	0.023	0.55
80	0.0235	0.6
70	0.024	0.65
60	0.0245	0.7
50	0.025	0.75
40	0.0255	0.8
30	0.026	0.85

Appendix-2. Detailed calculations

A.2.1. Design Example 1.

Solution.

An equal Maximum Bending Moment will occur at *C* and *D*.

M(applied) = 26.74 kNm

(i) **Step 1**

Assume an OPBF-strand reinforcement ratio of 5%.

Let the width of the beam $b = 150$ mm.

Let the total height of the beam be $h = 1.5b$ (i.e., 230 mm)

Preliminary sizing

$A_T = \rho bd$

Assuming a bar diameter of 30 mm and shear links of 8 mm, then effective depth d can be calculated as:

$d = h - 8 - 30$ (cover) $- 30/2 = 177$ mm

$A_T = 0.05$ x 150 x 177 $= 1328$ mm^2

(ii) **Step 2**

Modular ratio, $n = 0.813$

(iii) **Step 3**

Depth of the neutral axis (x)

$$\alpha = \sqrt{(n\rho)^2 + 2n\rho} - n\rho$$

$\alpha = 0.2473$

$x = \alpha d$

x = 43.78 mm

(iv) **Step 4**

Lever arm *(βd)*

Note: $\beta = 1 - (\alpha/3)$

$\beta d = 0.91757$ x 177 $= 162.4$ mm

(v) **Step 5**

Calculate stress in concrete and compare with the allowable stress ($0.45f_{ck}$)

$$f_c = \frac{2M}{b(\alpha d)(\beta d)}$$

$f_c = \frac{2 \text{ x } 26740000}{150 \text{ x } 43.78 \text{ x } 162.4} = 50.15$ *MPa*

50.15 MPa $> 0.45\, f_{ck}$…… NOT Ok!.

Similarly, stress in OPBF strands

$$f_T = \frac{M}{A_T \beta d}$$

$f_T = \frac{26740000}{1328 \text{ x } 162.4} = 124\ MPa$

124 MPa < 0.67 f_T ……. Ok!.

However, the section needs to be redesigned since allowable compressive stress in concrete is exceeded.

Possible adjustments.

Since the stress in the concrete is more critical, this controls the redesign.

Hence, the area of concrete can be increased by increasing the size of the section.

Let $b = 200$ mm.

Overall beam depth (h) = $2b = 400$.

$d = h$ – cover – $\Phi_{stirrup}$ – $0.5\Phi_T$.

$d = 400 – 40 – 8 – 12.5 – 15 = 320$ mm.

(Note that there will be 2 layers of reinforcement and the "12.5" is half of the 25 mm limit given by Eq. 28).

The new reinforcement ratio is 2.07%. This is less than the 2.88% recommendation from the experiments conducted in this study. Hence, we increase A_T.

Let $A_T = 2400$ mm^2.

Then $\rho = 3.75\%$.

Repeat ***Steps 3*** and ***4***.

Then:

Stress in concrete $f_c = 12.90$ MPa (OK).

Stress in OPBF strands $f_T = 37.55$ MPa (OK).

Provide 6 x 25Φ ($A_{T,prov} = 2944$ mm^2 strands as shown in Figure 11 and $sc = 47.5$, OK).

Based on the provided area of reinforcement ($\rho = 4.6\%$):

Stress in concrete $f_c = 11.89$ MPa (OK).

Stress in OPBF strands $f_T = 30.83$ MPa (OK).

Check for Shear.

Eurocode 2 provides a detailed procedure (Variable strut inclination method) for designing for shear as follows.

Check crushing strength of the diagonal concrete strut at the face of the beam support.

$V_{Rd,max} = 0.124 b_w d(1 - f_{ck}/250) f_{ck}$.

= 0.124 x 200 x 320 x (1 – 40/250) x 40.

= 267 kN (> $V_{Ed} = 56.3$ kN).

Therefore, stirrups are not required and the maximum longitudinal spacing of stirrup(s) can be calculated as:

s = minimum (0.75d or 600 mm).

Hence,

$s = 0.75$ x 320 = 240 mm.

Provide nominal shear reinforcement (e.g., T8 @ 250 mm spacing ($A_{sw} = 100$ mm^2))

$$\therefore \frac{A_{sw}}{s} = 0.4$$

Calculation of deflection.

Now, the long-term deflection can be calculated assuming that construction props are removed at 28 days.

Curvatures due to creep.

Step 1

(a) Calculate curvature due to uncracked section

$$\left(\frac{1}{r}\right)_{uc} = \frac{M}{E_{c,eff} I_{uc}}$$

To determine the creep coefficient,

Calculate the notional size (h_o) of the beam which is given by:

$h_o = 2A_c/u$ where A_c is the gross area of the section and u is its exposed perimeter. The h_o value is then used to determine the creep coefficient (φ) from Fig. 5b of Eurocode 2 presented in Fig. 8c.

h_o = (2 x 400 x 200)/1200 = 133.33 mm

and $\varphi = 2.0$.

Effective modulus is then determined as:

$$E_{c,eff} = \frac{E_{cm}}{(1 + \phi(\infty, t_0))},$$

$$E_{c,eff} = \frac{32}{(1+2)} = 10.67 \text{ GPa}.$$

Then the shrinkage due to the curvature of the uncracked section is:

$$\left(\frac{1}{r}\right)_{uc} = \frac{M}{E_{c,eff} I_{uc}},$$

$$\left(\frac{1}{r}\right)_{uc} = \frac{26.74\text{x}10^6}{10.67 \text{ x } 10^3 \text{ x } 200 \text{ x } \frac{400^3}{12}}$$

$$= \mathbf{2.35 \text{ x } 10\text{-}6 \text{ /mm}}$$

(b) Calculate curvature due to cracked section

(c) Depth of neutral axis $x = 76.34$ mm

$$I_{cr} = \frac{bx^3}{3} + nA_T(d-x)^2,$$

$$I_{cr} = \frac{200 \text{ x } 69.84^3}{3} + 0.813 \text{ x } 2400(320 - 69.78)^2,$$

$$I_{cr} = 1.72 \text{ x } 10^8 \ mm^4,$$

$$\left(\frac{1}{r}\right)_{cr} = \frac{M}{E_{c,eff} I_{cr}}$$

$$\left(\frac{1}{r}\right)_{cr} = \frac{26.74 \text{ x } 10^6}{10.67 \text{ x } 1.448 \text{ x} 10^8}$$

$$= \mathbf{1.46 \text{ x } 10^{-5} \text{ /mm}}$$

(d) Calculate "average" curvature due to uncracked and cracked section

$$\frac{1}{r} = \xi\left(\frac{1}{r}\right)_{cr} + (1-\xi)\left(\frac{1}{r}\right)_{uc},$$

where $\xi = 1 - \beta(M_{cr}/M)^2$

From elastic bending theory,

$$M_{cr} = f_{ctm} \text{ x } \frac{bh^2}{6}$$

f_{ctm} = tensile strength of the concrete = 3.5 MPa,

$$M_{cr} = 3.5 \text{ x } \frac{200 \text{ x } 400^2}{6} = 18.67 \ kNmm,$$

$$\xi = 1 - 0.5\ (18.67/26.74)^2,$$

$$\xi = 0.756,$$

$$\frac{1}{r} = 1.16 \text{ x } \frac{10^{-5}}{mm}.$$

Curvatures due to shrinkage.

Similarly, we determine the curvature of the uncracked and cracked sections. The formula for curvature due to shrinkage is

$$\frac{1}{r_{cs}} = \frac{\varepsilon_{cs}\alpha_e S}{I}.$$

Calculate curvature due to uncracked section

$$\frac{1}{r_{cs(un)}} = \frac{\varepsilon_{cs}\alpha_e S}{I_{uc}},$$

where

$$\varepsilon_{cs} = \varepsilon_{cd} + \varepsilon_{ca},$$

ε_{cd} = drying shrinkage strain,
ε_{ca} = autogenous shrinkage strain,

$$\varepsilon_{cd}\ (t) = \beta_{ds}\ \text{x}\ k_h\ \text{x}\ \varepsilon_{cd,0},$$

k_h = coefficient depending on the notional size of the section determined from Table 3.3 of Eurocode 2. $\varepsilon_{cd,0}$ is determined from Table 3.2 of Eurocode 2:

$$\beta_{ds} = \frac{t - t_s}{(t - t_s) + 0.04\sqrt{h_o^3}},$$

where t is the present age of the concrete, in days, t_s is the age of the concrete (days) at the beginning of drying shrinkage (or swelling), h is the notional size (mm) of the cross-section (with $h = 2A_c/u$).

$$\beta_{ds} = \frac{365 - 28}{(365 - 28) + 0.04\sqrt{133.33^3}} = 0.845.$$

By interpolation from Table 2, $k_h = 0.95$.
Hence drying shrinkage at 365 days at 80% humidity; $\left(\varepsilon_{cd,0} = 0.0024\right)$.

$$\varepsilon_{cd}\quad (t) = \beta_{ds}\ \text{x}\ k_h\ \text{x}\ \varepsilon_{cd,0},$$

ε_{cd} (1 year) = 0.845 x 0.95 x 0.0024 = 0.0019266,
Autogenous shrinkage strain is given as.
$\varepsilon_{ca}(t) = \beta_{as}(t)\varepsilon_{ca}(\infty)$, where.
$\varepsilon_{ca}(\infty) = 2.5\left(f_{ck} - 10\right)\text{x}10^{-6}$and.
$\beta_{as}(t) = 1 - \exp\left(-0.2t^{0.5}\right)$ where t is in days.
Therefore

$$\beta_{as}(365) = 1 - \exp\left(-0.2\text{x}365^{0.5}\right) = 0.978,$$

$$\varepsilon_{ca}(\infty) = 2.5(30 - 10)\text{x}10^{-6} = 0.00005,$$

$\varepsilon_{ca}(t) = 0.978$ x $0.00005 = 0.0000489$,

$$\varepsilon_{cs} = 0.0019266 + 0.0000489 = 0.001976,$$

We now have all the respective parameters except S, the first moment of area of reinforcement about the centroid of the section

$$\frac{1}{r_{cs(un)}} = \frac{\varepsilon_{cs}\alpha_e S}{I_{uc}}.$$

$S = A_T\ (d - x)$;

$$\frac{1}{r_{cs(un)}} = \frac{0.001976\ \text{x}\ 0.813\ \text{x}\ 2944\left(320 - \frac{400}{2}\right)}{200\ \text{x}\ 400^3}$$

$$= 5.32\ \text{x}\ \frac{10^{-7}}{mm}.$$

- Calculate curvature due to cracked section

$$\frac{1}{r_{cs(cr)}} = \frac{\varepsilon_{cs}\alpha_e S}{I_{cr}},$$

$$\frac{1}{r_{cs(cr)}} = \frac{0.0019755\ \text{x}\ 0.813\ \text{x}\ 2944\ (320 - 76.34)}{171673102}$$

$$= 6.71\text{x}\frac{10^{-6}}{mm}.$$

- Calculate “average” curvature due to uncracked and cracked section.

$$\frac{1}{r_{cs}} = \xi\left(\frac{1}{r}\right)_{cs(cr)} + (1-\xi)\left(\frac{1}{r}\right)_{cs(uc)},$$

$$\frac{1}{r_{cs}} = 0.756(6.71e-6) + (1-0.756)(5.32e-7)$$

$$= 5.2 \text{ x } \frac{10^{-6}}{mm}$$

- Total curvature = curvature due to loading (creep) + curvature due to shrinkage

Curvature due to creep $= 1.16\text{x}10^{-5}/\text{mm}$
Curvature due to shrinkage $= 5.20\text{x}10^{-6}/mm$
Total curvature $= 1.68\text{x}10^{-5}/mm$
From the generic formula for deflection (Eq. 9),

$$\delta_{max} = \frac{1}{r}kL^2$$

For a simply supported beam with the loading arrangement in this design example (Fig. 8), $k = 0.103$

$$\delta_{max} = 1.68 \text{ x } \frac{10^{-5}}{mm} \text{x } 0.103 \text{ x } (1300)^2 \ mm^2 = 2.93 \ mm$$

The calculated deflection is less than the limit specified in Eurocode 2 (span/250) which in this case is 5.2 mm (hence deflection is OK!).

A.2.2. Design Example 2.

Solution.

The beam breadth b will match the wall thickness so that.
$b = 230$ mm.
Assuming a concrete weight of 24 kN/m^3 a beam dead weight of about 14 kN can be assumed, so that the ultimate load is:
$F = 114 + 40 = 154$ kN.
The shear force.
$V = 77$ kN.
For the assumed triangular load distribution for the preliminary analysis, we have

$$M = \frac{F \text{ x } span}{6} = 103 \text{ kNm}$$

Step 1.
Assume a reinforcement ratio of 8.6%.
Hence, $A_T = 10{,}500$ mm^2.
Let the total height of the beam be $3b$ (i.e., 690 mm).
Preliminary sizing.
$A_T = \rho bd$.
Assuming a strand diameter of 30 mm, then we need 15 strands in 5 layers. Let cover be 25 mm, then an overall section depth h of 715 mm should suffice, while effective depth d is 530 mm.

Step 2.
$n = 0.839$.
Steps 3 and **4.**
$\alpha = 0.316$.
$x = 0.316 \text{ x } 530 = 167.48$ mm.
Then:
Stress in concrete $f_c = 11.32$ MPa (< 13.5 MPa ……. OK).
Stress in OPBF strands $= 20.67$ MPa (< 165 MPa ……OK).
Provide 15 x 30Φ_T ($A_{T,prov} = 10598$ mm^2) strands (Fig. 12).

Check for Shear.

Eurocode 2 provides a detailed procedure (Variable strut inclination method) for designing for shear.
Check crushing strength of the diagonal concrete strut at the face of the beam support.
$V_{Rd,max} = 0.124 b_w d\ (1 - f_{ck}/250)\ f_{ck}$.
$= 0.124 \text{ x } 230 \text{ x } 530 \text{ x } (1 - 30/250) \text{ x } 30.$
$= 399$ kN ($> V_{Ed} = 77$ kN).
∴ stirrups are not required and the maximum longitudinal spacing of stirrup (s) can be calculated as:

s = minimum (0.75d or 600 mm).
Hence,
s = 0.75 x 530 = 397.5 mm.
But the maximum spacing for beams provided for in the Eurocode 2 is 300 mm.
Provide nominal shear reinforcement (e.g., T8 @ 300 mm spacing: A_{sw} = 100 mm^2)

Therefore, $\frac{A_{sw}}{s} = 0.333$

Calculation of Deflection.
Following the methods described in design example 1,

(i) **Effect of loading on curvature due to creep**
Creep coefficient $\varphi = 1.9$

$$E_{c,eff} = \frac{E_{cm}}{(1+\phi(\infty, t_0))}$$

$$E_{c,eff} = \frac{31}{(1+1.9)} = 10.69 \text{ GPa}$$

Curvature (of uncracked section) = 1.405 x 10^{-6} /mm
Curvature (of cracked section) = 6.305 x 10^{-6} /mm
Average curvature (1/r) is:

$$\frac{1}{r} = \xi\left(\frac{1}{r}\right)_{cr} + (1-\xi)\left(\frac{1}{r}\right)_{uc},$$

$$where \quad \xi = 1 - \beta(M_{cr}/M)^2$$

M_{cr} = 50.24 kNm
Therefore, ξ = 0.8810
Average curvature ($1/r$) = 5.722 x 10^{-6} /mm

(ii) **Effect of loading on curvature due to Shrinkage**

Uncracked section.

$$\frac{1}{r_{cs(un)}} = \frac{\varepsilon_{cs}\alpha_e S}{I_{uc}},$$

Recall, $\varepsilon_{cs} = \varepsilon_{cd} + \varepsilon_{ca}$
ε_{cd} (drying shrinkage strain) = 0.0021.
ε_{ca} (autogenous shrinkage strain) = 3.668 x 10^{-5}.
ε_{cd} (365 $days$) = β_{ds} x k_h x $\varepsilon_{cd,0}$ = 0.7863 x 0.891 x 0.003.k_h (coefficient depending on the notional size of the section determined from) = 0.891.
S (of uncracked section) = 1854650 mm^3.
Therefore curvature (of uncracked section) = 4.850 x 10^{-7} /mm.
Cracked section

$$\frac{1}{r_{cs(cr)}} = \frac{\varepsilon_{cs}\alpha_e S}{I_{cr}}$$

I_{cr} = 1.53 x 10^9 mm^4.
S (of cracked section) = 3842744 mm^3.
Therefore curvature (of cracked section) = 4.511 x 10^{-6} /mm.
Average Curvature

$$\frac{1}{r_{cs}} = \xi\left(\frac{1}{r}\right)_{cs(cr)} + (1-\xi)\left(\frac{1}{r}\right)_{cs(uc)}$$

= 0.881 (4.511 x 10^{-6}) + [(1 – 0.881) x (4.850 x 10^{-7})].
= 4.032 x 10^{-6} /mm.
Total curvature = 5.722 x 10^{-6} + 4.032 x 10^{-6}.
= 9.753 x 10^{-6} /mm.

Deflection (δ_{max}) from Eq. 9.

$$\delta_{max} = \frac{1}{r} kL^2$$

For the load pattern on the beam, $k = 0.100$, hence.
$\delta_{max} = 9.753 \text{ x } 10^{-6} \text{ x } 0.100 \text{ x } 4000^2$.
$= 15.61$ mm (which is less than 4000/250 OK).

A.2.3. Design Example 3.

Solution (uncracked section).

A sketch of the beam is provided in Fig. 10a thus:
Maximum moment will occur at midspan.
$M = wL^2/8 = 46 \text{ x } 3.5^2/8$.
$= 70.4$ kNm.

Step 1.

Assume a reinforcement ratio of 4.8%.
Let the width of the beam be 230 mm.
Let the total height of beam be 550 mm.

Preliminary sizing.

$A_T = \rho bd$.
Assuming a bar diameter of 30 mm and shear links of 8 mm, then effective depth d can be calculated as $d = h - 8 - 30$ (cover) $- 30/2 = 450$ mm.
$A_T = 0.0483 \text{ x } 230 \text{ x } 450 = 5000 \text{ mm}^2$.

Step 2.

Modular ratio, $n = 0.926$.

Step 3.

Determine the depth of the neutral axis (x)

$$\alpha = \sqrt{(n\rho)^2 + 2n\rho} - n\rho$$

$\alpha = 0.2577$.
$x = \alpha d$.
$x = 116$ mm.

Step 3.

Calculate Lever Arm (βd).
$\beta = 1 - (\alpha/3)$.
$\beta d = 0.9141 \text{ x } 450 = 411.3$ mm.

Step 4.

Calculate stress in concrete and compare with the allowable stress ($0.45 f_{cu}$).

$$f_c = \frac{2M}{b(\alpha d)(\beta d)}$$

$f_c = \frac{2 \text{ x } 26740000}{150 \text{ x } 43.78 \text{ x } 162.4} = 12.83\ MPa$
$12.83 MPa < f_{c,all}$.....**Ok**!
Similarly, stress in OPBF strands is calculated:

$$f_T = \frac{M}{A_T \beta d}$$

Stress in OPBF strands $f_T = 34.23$ MPa $< f_{T,all}$ .....**Ok!**.
Provide 6 x 35Φ_T strands as shown in Fig. 13 ($A_{T,prov} = 5767 \text{ mm}^2$ and $sc = 47.5$ mm, OK):
Based on the provided area of reinforcement ($\rho = 4.73\%$):
Stress in concrete $f_c = 12.39$ MPa (OK).
Stress in OPBF strands $f_T = 33.45$ MPa (OK).

Check for shear.

Eurocode 2 provides a detailed procedure (Variable strut inclination method) for designing for shear.
Check crushing strength of the diagonal concrete strut at the face of the beam support.
$V_{Rd,max} = 0.124 b_w d(1 - f_{ck}/250) f_{ck}$.
$= 0.124 \text{ x } 230 \text{ x } 460 \text{ x } (1 - 30/250) \text{ x } 30$.
$= 346$ kN ($> V_{Ed} = 80.5$ kN).
Therefore, stirrups are not required and the maximum longitudinal spacing of stirrup (s) can be calculated as:
$s =$ minimum ($0.75d$ or 600 mm).
$s = 0.75 \text{ x } 460 = 345$ mm.

Provide nominal reinforcement (e.g., T8 @ 300 mm spacing: $A_{sw} = 100$ mm^2)

$$\therefore \frac{A_{sw}}{s} = 0.33$$

Solution (cracked section).
Moment capacity of section

$$M = \frac{fI}{y}$$

Where f is the allowable material strength, I is the moment of inertia of the section (in this case, concrete is cracked), and y is the depth of the neutral axis.

$$I_{cracked} = \frac{bx^3}{3} + nA_T(d-x)^2,$$

$$I_{cracked} = \frac{230 \times 124.7^3}{3} + 0.926 \times 5765\ (460 - 124.7)^2 = 748.8 \times 10^6 \quad \text{mm}^4$$

Therefore,
Cracked Moment Capacity.
$M = \frac{13.5 \text{ x } 748.8 \text{ x } 10^6}{124.7} = \boldsymbol{81.1}$ kNm (as required)
Calculation of deflection.
Following the methods described in design example 1.
Effect of loading on curvature due to creep.
Creep coefficient $\varphi = 2.8$,

$$E_{c,eff} = \frac{E_{cm}}{(1 + \phi(\infty, t_0))}$$

$$E_{c,eff} = \frac{27}{(1 + 2.8)} = 7.11\text{GPa}$$

Curvature (of uncracked section) = 1.180 x 10^{-6} /mm.
Curvature (of cracked section) = 5.025 x 10^{-6} /mm.
Average curvature ($1/r$)

$$\frac{1}{r} = \xi\left(\frac{1}{r}\right)_{cr} + (1-\xi)\left(\frac{1}{r}\right)_{uc}$$

$$where \quad \xi = 1 - \beta(M_{cr}/M)^2$$

$M_{cr} = 33.63$ kNm.
Therefore, $\xi = 0.2092$.
Average curvature ($1/r$) = 1.985 x 10^{-6} /mm.
Effect of loading on curvature due to shrinkage.
Uncracked section

$$\frac{1}{r_{cs(un)}} = \frac{\varepsilon_{cs}\alpha_e S}{I_{uc}}$$

$$where \quad \varepsilon_{cs} = \varepsilon_{cd} + \varepsilon_{ca}$$

ε_{cd} (drying shrinkage strain) = 0.0022.
ε_{ca} (autogenous shrinkage strain) = 4.890 x 10^{-5}.
$\varepsilon_{cd}\ \ (365days) = \beta_{ds}xk_hx\varepsilon_{cd,0}$ = 0.8031 x 0.907 x 0.003k_h (coefficient depending on the notional size of the section) = 0.907.
S (uncracked section) = 1066895 mm^3.
Therefore curvature (uncracked section) = 6.921 x 10^{-7} /mm.
Uncracked section

$$\frac{1}{r_{cs(cr)}} = \frac{\varepsilon_{cs}\alpha_e S}{I_{cr}}$$

$I_{cr} = 7.49$ x 10^8 mm^4.
S (cracked section) = 1933306 mm^3.
Therefore curvature (cracked section) = 5.340 x 10^{-6} /mm.

Average curvature

$$\frac{1}{r_{cs}} = \xi\left(\frac{1}{r}\right)_{cs(cr)} + (1-\xi)\left(\frac{1}{r}\right)_{cs(uc)}$$

$= 0.209\ (1.985 \times 10^{-6}) + [(1 - 0.209) \times (6.921 \times 10^{-7})]$.
$= 1.665 \times 10^{-6}$ /mm.
Total curvature $= 1.980 \times 10^{-6} + 1.665 \times 10^{-6}$.
$= 3.649 \times 10^{-6}$ /mm.
Deflection (δ_{max}) from Eq. 9.

$$\delta_{max} = \frac{1}{r} \quad kL^2$$

For the load pattern on the beam, k = 0.104, hence.
$\delta_{max} = 3.649 \times 10^{-6} \times 0.104 \times 3500^2$.
= 4.65 mm (which is less than 3500/250 mm OK).

References

[1] A. Bras, C. Ravijanya, V. Torres de Sande, M. Riley, R.V. Ralegaonkar, Sustainable and affordable prefab housing systems with minimal whole life energy use, Energy Build. (2020) 110030.
[2] J. Claramunt, L.J. Fernández-Carrasco, H. Ventura, M. Ardanuy, Natural fiber nonwoven reinforced cement composites as sustainable materials for building envelopes, Constr. Build. Mater. vol. 115 (2016) 230–239.
[3] L. Chen, Z. Chen, Z. Xie, L. Wei, J. Hua, L. Huang, P.-S. Yap, Recent developments on natural fiber concrete: A review of properties sustainability, applications, barriers, and opportunities, Dev. Built Environ. vol. 16 (2023) 100255.
[4] S.N. Chinnu, S.N. Minnu, A. Bahurudeen, R. Senthilkumar, Recycling of industrial and agricultural wastes as alternative coarse aggregates: a step towards cleaner production of concrete, Constr. Build. Mater. (2021) 123056.
[5] X. Cao, X. Dai, J. Liu, Building energy-consumption status worldwide and the state-of-the-art technologies for zero-energy buildings during the past decade, Energy Build. vol. 128 (198-213) (2016) 198–213.
[6] P. Capros, A. De Vita, N. Tasios, D. Papadopoulos, P. Siskos, E. Apostolaki, M. Zampara, L. Paroussos, K. Fragiadakis and N. Kouvaritakis, EU energy, transport and GHG emissions: trends to 2050 - reference scenario, European Union, Luxembourg, 2013.
[7] J. Page, F. Khadraoui, M. Boutouil, M. Gomina, Multi-physical properties of a structural concrete incorporating short flax fibers, Constr. Build. Mater. vol. 140 (2017) 344–353.
[8] F. Asdrubali, F. D'Alessandro, S. Schiavoni, A review of unconventional sustainable building insulation materials, Sustain. Mater. Technol. vol. 4 (2015) 1–17.
[9] E.O. Momoh, A.I. Osofero, O. Menshykov, Enhancing the behaviour of broom-strands reinforced concrete using hose-clamps, Mater. Today.: Proc. vol. 65 (2022) 572–580.
[10] A. Bras, C. Ravijanya, V. Torres de Sande, M. Riley, R.V. Ralegaonkar, Sustainable and affordable prefab housing systems with minimal whole life energy use, Energy Build. vol. 220 (2020) 110030.
[11] O.S. Ogbo, E.O. Momoh, E.E. Ndububa, O.O. Afolayan, S. Onuche, J.O. Agada, Scheffe's polynomial optimisation of laterite concrete incorporating periwinkle shells and coir, KSCE J. Civ. Eng. (2023).
[12] Y. Tang, Y. Wang, D. Wu, M. Chen, L. Pang, J. Sun, W. Feng, X. Wang, Exploring temperature-resilient recycle daggregate concrete with waste rubber: an experimental and multi-objective optimization analysis, Rev. Adv. Mater. Sci. vol. 62 (2023) 20230347.
[13] A. Singh, Y. Wang, Y. Zhou, J. Sun, X. Xu, Y. Li, Z. Liu, J. Chen, X. Wang, Utilization of antimony tailings in fiber-reinforced 3D printed concrete: a sustainable approach for construction materials, Constr. Build. Mater. vol. 408 (2023) 133689.
[14] H. Huang, Y. Yuan, W. Zhang, L. Zhu, Property assessment of high-performance concrete containing three types of fibers, Int. J. Concr. Struct. Mater. vol. 15 (39) (2021) 1–17.
[15] M. Duque-Acevedo, L.J. Belmonte-Ureña, F.J. Cortés-García, F. Camacho-Ferrea, Agricultural waste: review of the evolution, approaches and perspectives on alternative uses, Glob. Ecol. Conserv. vol. 22 (2020) e00902.
[16] I. Uchegbulam, E.O. Momoh, S.A. Agan, Potentials of palm kernel shell derivatives: a critical review on waste recovery for environmental sustainability, Clean. Mater. vol. 6 (2022) 100154.
[17] M. Arun, K. Basker, B.S. Geethapriya, M. Jayabarathi, R. Angayarkkani, Affordable housing: cost effective construction materials for economically weaker section, Mater. Today.: Proc. vol. 45 (2021) 7838–7844.
[18] O. Onuaguluchi, N. Banthia, Plant-based natural fibre reinforced composites: a review, Cem. Concr. Compos. vol. 68 (2016) 96–108.
[19] M. Ardanuy, J. Claramunt, R.D. Toledo Filho, Cellulosic fiber reinforced cement-based composites: a review of recent research, Constr. Build. Mater. vol. 79 (2015) 115–128.
[20] H.A. Colorado, A. Loaiza, Portland Cement Paste Blended with Pulverized Coconut Fibers, in: T. Ohji, J. Matyas, H. Colorado, R. Kanakala (Eds.), Advances in Materials Science for Environmental and Energy Technologies VI, vol. 262, The American Ceramic Society, 2017, pp. 79–84.
[21] V. Agopyan, H. Savastano Jr, V.M. John, M.A. Cincotto, Developments on vegetable fibre–cement based materials in São Paulo, Brazil: an overview, in: Cement and Concrete Composites, vol. 27, 2005, pp. 527–536.
[22] P. Lertwattanaruk, A. Suntijitto, Properties of natural fiber cement materials containing coconut coir and oil palm fibers for residential building applications, Constr. Build. Mater. vol. 94 (2015) 664–669.
[23] E.O. Momoh, B.I.O. Dahunsi, Suitability of oil-palm-broom-fibres as reinforcement for laterite-based roof tiles, Int. J. Softw. Hardw. Res. Eng. vol. 5 (4) (2017) 27–35.
[24] N. Benmansour, B. Agoudjil, A. Gherabli, A. Kareche, A. Boudenne, Thermal and mechanical performance of natural mortar reinforced with date palm fibers for use as insulating materials in building, Energy Build. vol. 81 (2014) 98–104.
[25] H.P.S. Abdul Khalil, M. Jawaid, A. Hassan, M.T. Paridah, A. Zaidon, Oil palm biomass fibres and recent advancement in oil palm biomass fibres based hybrid biocomposites, Compos. Appl. (2012) 187–220.
[26] R. Nadlene, S.M. Sapuan, M. Jawaid, M.R. Ishak, L. Yusriah, A review on roselle fiber and its composites, J. Nat. Fibers vol. 13 (1) (2015) 10–41.
[27] M.S. Sreekala, J. George, M.G. Kumaran, S. Thomas, The mechanical performance of hybrid phenol-formaldehyde-based composites reinforced with glass and oil palm fibres, Compos. Sci. Technol. vol. 62 (3) (2002) 339–353.
[28] R. Dungani, M. Jawaid, H.P.S. Abdul Khalil, J. Jasni, S. Aprilia, K.R. Hakeem, S. Hartati, M.N. Islam, A review on quality enhancement of oil palm trunk waste by resin impregnation: future materials, BioResources vol. 8 (2) (2013) 3136–3156.

[29] A.V. Kiruthika, A review on physico-mechanical properties of bast fibre reinforced polymer composites, J. Build. Eng. vol. 9 (2016) 91–99.
[30] H. Khalel, M. Khan, A. Starr, K.A. Khan, A. Muhammad, Performance of engineered fibre reinforced concrete (EFRC) under different load regimes: a review, Constr. Build. Mater. vol. 306 (2021) 124692.
[31] B. Fu, K.C. Liu, J.F. Chen, J.G. Teng, Concrete reinforced with macro fibres recycled from waste GFRP, Constr. Build. Mater. vol. 310 (2021) 125063.
[32] S.K. Loh, The potential of the Malaysian oil palm biomass as a renewable energy source, Energy Convers. Manag. vol. 141 (2017) 285–298.
[33] E.O. Momoh, A.I. Osofero, Recent developments in the application of oil palm fibers in cement composites, Front. Struct. Civ. Eng. vol. 14 (2020) 94–108.
[34] M. Muhtar, S.M. Dewi, Wisnumurti, A. Munawir, Enhancing bamboo reinforcement using a hose-clamp to increase bond-stress and slip resistance, J. Build. Eng. vol. 26 (2019) 100896.
[35] N. Ganesan, P.V. Indira, P.R. Himasree, Bamboo reinforced concrete wall panels under one way in-plane action, Environ., Dev. Sustain. vol. 22 (2020) 1475–1488.
[36] E.O. Momoh, A.I. Osofero, O. Menshykov, Behaviour of clamp-enhanced palm tendon reinforced concrete, Constr. Build. Mater. vol. 341 (2022) 127824.
[37] E.O. Momoh, B.I.O. Dahunsi, Suitability of oil-palm-broom-fibres as reinforcement for laterite-based roof tiles, Int. J. Softw. Hardw. Res. Eng. vol. 5 (4) (2017) 27–35.
[38] E.O. Momoh, A.I. Osofero, A. Martinez-felipe, F. Hamzah, Physico-mechanical behaviour of Oil Palm Broom Fibres (OPBF) as eco-friendly building material, J. Build. Eng. vol. 30 (2020) 101208.
[39] E.O. Momoh, A.I. Osofero, Behaviour of oil palm broom fibres (OPBF) reinforced concrete, Constr. Build. Mater. vol. 221 (2019) 745–761.
[40] E.O. Momoh, A.I. Osofero, O. Menshykov, Bond behaviour of oil palm broom fibres in concrete for eco-friendly construction, Constr. Mater. vol. 174 (1) (2021) 47–64.
[41] E.O. Momoh, A.I. Osofero, O. Menshykov, Physicomechanical properties of treated oil palm-broom fibers for cementitious composites, J. Mater. Civ. Eng. vol. 32 (2020) 04020300.
[42] E.O. Momoh, A.I. Osofero, O. Menshykov, Bond behaviour of treated natural fibre in concrete, Nano Hybrids Compos. vol. 34 (2022) 37–44.
[43] Y. Nie, Y. Wei, K. Miao, K. Zhao, L. Huang, Experimental investigation of full-culm bamboo tubes strengthened by filled concrete and bamboo sheets under axial compression, J. Build. Eng. vol. 45 (2022) 103548.
[44] W. Shangguan, Y. Zhong, X. Xing, R. Zhao, H. Ren, Strength models of bamboo scrimber for compressive properties, J. Wood Sci. vol. 61 (2015) 120–127.
[45] H. Li, S. Shen, The mechanical properties of bamboo and vascular bundles, J. Mater. Res. vol. 26 (21) (2011) 2749–2756.
[46] M. Xu, Z. Cui, L. Tu, Q. Xia, Z. Chen, The effect of elevated temperatures on the mechanical properties of laminated bamboo, Constr. Build. Mater. vol. 226 (2019) 32–43.
[47] X. Zhang, Z. Yu, Y. Yu, H. Wang, J. Li, Axial compressive behavior of Moso Bamboo and its components with respect to fiber-reinforced composite structure, J. For. Res. vol. 30 (2019) 2371–2377.
[48] K. Ghavami, Ultimate load behaviour of bamboo-reinforced lightweight concrete beams, Cem. Concr. Compos. vol. 17 (4) (1995) 281–288.
[49] Eurocode-2, "EN 1992–1-1: Design of concrete structures - Part 1–1: General rules and rules for buildings," The European Union Per Regulation 305/2011, Directive 98/34/EC, Directive 2004/18/EC, 2004.
[50] R. Qin, A. Zhou, D. Lau, Effect of reinforcement ratio on the flexural performance of hybrid FRP reinforced concrete beams, Compos. Part B: Eng. vol. 108 (2017) 200–209.
[51] H. Archila, S. Kaminski, D. Trujillo, E.Z. Escamilla, K.A. Harries, Bamboo reinforced concrete: a critical review, Mater. Struct. vol. 51 (102) (2018) 1–18.
[52] S.Y. Kute, M.R. Wakchaure, Performance evaluation for enhancement of some of the engineering properties of bamboo as reinforcement in concrete, J. Inst. Eng. (India): Ser. A vol. 94 (4) (2013) 235–242.
[53] ACI 361R: 1986, "Composite concrete and steel high-pressure vessels for general industrial use," American Concrete Institute, 2013.
[54] J. Lubliner, J. Oliver, S. Oller, E. Onate, A plastic-damage model for concrete, Int. J. Solids Struct. vol. 25 (3) (1989) 299–326.
[55] B.L. Wahalathantri, D.P. Thambiratnam, T.H.T. Chan and S. Fawzia, "A material model for flexural crack simulation in reinforced concrete elements using ABAQUS," in *Infrastructure, Transport and Urban Development, eddBE2011 Proceedings*, Brisbane, Australia, 2011.
[56] J. Lee, G.L. Fenves, Plastic-damage model for cyclic loading of concrete structures, J. Eng. Mech. vol. 124 (8) (1998) 892–900.
[57] B. Zhou, R. Wu, S. Lu, S. Yin, A general numerical model for predicting the flexural behavior of hybrid FRP-steel reinforced concrete beams, Eng. Struct. vol. 239 (2021) 112293.
[58] A.S. Genikomsou, M.A. Polak, Finite element analysis of punching shear of concrete slabs using damaged plasticity model in ABAQUS, Eng. Struct. vol. 98 (1) (2015) 38–48.
[59] D.A. Gujel, C.S. Kazmierczak, J.R. Masuero, Stress-strain curve of concretes with recycled concretea ggregates: analysis of the NBR 8522 methodology, Ibracon Struct. Mater. J. vol. 10 (3) (2017) 547–567.
[60] P. Bamforth, D. Chisholm, J. Gibbs and T. Harrison, "Properties of concrete for use in eurocode 2," The Concrete Centre, Surrey, UK, 2008.
[61] M. Al-Huri, S. Ahmad, M. Al-Osta, A. Al-Gadhib and M. Kalimur Rahman, "Numerical investigation of RC beam strengthened with UHPFRC layers using cohesive surface bonding method," in *Fifth Conference on Smart Monitoring, Assessment and Rehabilitation of Civil Structures*, Potsdam, Germany, 2019.
[62] V. Alizadeh, Finite element analysis of controlled low strength materials, Front. Struct. Civ. Eng. vol. 13 (5) (2019) 1243–1250.
[63] P.P. Camanho, C.G. Dávila, Mixed-Mode Decohesion Finite Elements for the Simulation of Delamination in Composite Materials, NASA,, Hampton, VA, USA, 2002.
[64] F. Liravi, S. Das, C. Zhou, Separation force analysis and prediction based on cohesive element model for constrained-surface Stereolithography processes, Comput. -Aided Des. vol. 69 (2015) 134–142.
[65] A. Ali, A. Lo Conte, C.A. Biffi, A. Tuissi, Cohesive surface model for delamination and dynamic behavior of hybrid composite with SMA-GFRP interface, Int. J. Lightweight Mater. Manuf. vol. 2 (2) (2019) 146–155.
[66] M. Ramamurthi, J.-S. Lee, S.-H. Yang, Y.-S. Kim, Delamination characterization of bonded interface in polymer coated steel using surface based cohesive model, Int. J. Precis. Eng. Manuf. vol. 14 (2013) 1755–1765.
[67] R.D.S.G. Campilho, M.F.S.F. de Moura, J.J.M.S. Domingues, Using a cohesive damage model to predict the tensile behaviour of CFRP single-strap repairs, Int. J. Solids Struct. vol. 45 (5) (2008) 1497–1512.
[68] "Concrete Industry Sustainability Performance Report: 12th report: 2018 performance data," MPA The Concrete Centre, London, 2020.
[69] A. Hasanbeigi, M. Arens, J.C.R. Cardenas, L. Price, R. Triolo, Comparison of carbon dioxide emissions intensity of steel productionin China, Germany, Mexico, and the United States, Resour., Conserv. Recycl. vol. 113 (2016) 127–139.
[70] L. Yang, C. Hao, Y. Chai, Life cycle assessment of commercial delivery trucks: diesel, plug-in electric, and battery-swap electric, Sustainability vol. 10 (2018) 1–21.
[71] A. Mishra, F. Humpenöder, G. Churkina, C.P.O. Reyer, F. Beier, B.L. Bodirsky, H.J. Schellnhuber, H. Lotze-Campen, A. Popp, Land use change and carbon emissions of a transformation to timber cities, Nat. Commun. vol. 13 (2022) 4889.
[72] D.B. Müller, G. Liu, A.N. Løvik, R. Modaresi, S. Pauliuk, F.S. Steinhoff, H. Brattebø, Carbon emissions of infrastructure development, Environ. Sci. Technol. vol. 47 (20) (2013) 11739–11746.